The Opto-inflammasome in zebrafish: a tool to study cell and tissue responses to speck formation and cell death

Eva Hasel de Carvalho[1], Shivani Dharmadhikari[1], Kateryna Shkarina[2], Jingwei Rachel Xiong[3], Bruno Reversade[4,5,6,7], Petr Broz[2], Maria Leptin[1]

[1] European Molecular Biology Laboratory (EMBL), Directors' Research, Meyerhofstrasse 1, 69117 Heidelberg, Germany
[2] Department of Biochemistry, University of Lausanne, Epalinges, Switzerland
[3] Skin Research Laboratories (ASRL), A*STAR, Singapore
[4] Institute of Molecular and Cell Biology (IMCB), A*STAR, Singapore, Singapore.
[5] Department of Pediatrics, National University of Singapore (NUS), Singapore, Singapore.
[6] Medical Genetics Department, Koç University School of Medicine (KUSOM), Istanbul, Turkey.
[7] Laboratory of Human Genetics & Therapeutics, Genome Institute of Singapore (GIS), A*STAR, Singapore, Singapore.

The inflammasome is a conserved system for the intracellular detection of danger or pathogen signals. By forming a large intracellular multiprotein signaling platform, it activates downstream effectors that initiate a rapid necrotic programmed cell death (PCD) termed pyroptosis and activation and secretion of pro-inflammatory cytokines to warn and activate surrounding cells. However, inflammasome activation is difficult to control on a single-cell level using canonical triggers. We constructed Opto-Asc, a light-responsive form of the inflammasome adaptor protein ASC (Apoptosis-Associated Speck-Like Protein Containing a CARD) which allows tight control of inflammasome formation *in vivo*.

We introduced a cassette of this construct under the control of a heat shock element into zebrafish in which we can now induce Asc inflammasome (speck) formation in single cells of the skin.

We find that cell death resulting from Asc speck formation is morphological distinct from apoptosis in periderm but not in basal cells. Asc induced PCD in can lead to apical or basal extrusion from the periderm. The apical extrusion in periderm cells depends on Caspb but and triggers a strong Ca^{2+} signaling response in nearby cells.

33 ## Introduction

34 The innate immune system plays a crucial role in early recognition and eradication of
35 potentially dangerous microorganisms. Inflammasomes are among the best characterized
36 components of innate antimicrobial defense in vertebrates. Inflammasome activation is
37 induced following recognition of pathogen-associated molecular patterns (PAMPs) or
38 danger-associated molecular patterns (DAMPs) by intracellular pattern-recognition
39 receptors, such as NOD-like receptors (NLRs) and AIM2-like receptors (ALRs). This leads to
40 the formation of the large multiprotein platforms, which often contain the adaptor molecule
41 ASC (apoptosis-associated speck-like protein containing a CARD), that in turn recruit and
42 activate proinflammatory caspases (Martinon, Burns and Tschopp, 2002). These caspases
43 cleave and thereby activate downstream effector molecules, including the pore-forming
44 Gasdermins (GSDMs) and pro-inflammatory cytokines such as interleukin-1β (IL-1β) and
45 interleukin-18 (IL-18), which are then released through the GSDM pores (Evavold *et al.*,
46 2018; Heilig *et al.*, 2018)
47 Inflammasome pathway components are expressed in immune and non-immune cells, but
48 have been studied extensively mostly in cultured cells or bone marrow derived
49 macrophages (Tweedell, Malireddi and Kanneganti, 2020). Recent studies also highlight their
50 involvement in antimicrobial defense of epithelial tissues (Santana *et al.*, 2016; Churchill,
51 Mitchell and Rauch, 2022).
52 Epithelia are the first point of contact between the host organism and microbial invaders.
53 Although the role of inflammasome components can be studied *in vivo* using epithelial
54 infection models, little is known about the direct effects of inflammasome formation on cells
55 and their neighbors in the context of the live tissue. Thus, analysis of this dynamic and rapid
56 process would benefit from precise spatial control of inflammasome formation and live
57 imaging of the ensuing physiological events.
58 Zebrafish are well suited to study innate and adaptive immunity *in vivo* (Novoa and Figueras,
59 2012; Renshaw and Trede, 2012). Their fast development, their transparency in early stages
60 and a multitude of fluorescent reporter lines offer ideal conditions for real-time visualization
61 of cellular processes in tissues. Some of the genes encoding core components of innate
62 immune signaling pathways are highly conserved in the zebrafish (Stein *et al.*, 2007), while
63 others, like those encoding the fish-specific NLR proteins, are more divergent (Howe *et al.*,
64 2016). The adaptor protein ASC is among the most highly conserved inflammasome

65 components in all vertebrates. ASCconsists of a pyrin domain (PYD) and a caspase
66 recruitment domain (CARD) connected by a flexible linker. Once activated, ASCsc undergoes
67 prion-like oligomerization, concentrating the entire pool of ASC in the cell in one spot to
68 form a dense fibrous structure termed the ASCsc-speck (Dick et al., 2016).
69 In zebrafish, Asc is expressed both in epithelial and immune cells, such as macrophages and
70 neutrophils (Kuri et al., 2017). The larval zebrafish skin consists of two cell layers. The outer
71 cell layer, periderm, consists of keratinocytes which show characteristic actin ridges and are
72 tightly connected, the underlying layer consists of basal cells which in adult zebrafish harbor
73 a stem cell pool to replace dying cell in the skin (Lee, Asharani and Carney, 2014). During
74 larval development the periderm is gradually replaced and until then grows by divisions and
75 asymmetric fission (Chan *et al.*, 2022).A functional inflammasome can be induced in both
76 layers of the larval zebrafish skin by over-expressing Asc-mKate2, leading to immediate cell
77 death of periderm and basal cells, (Kuri et al., 2017).
78 Similarly to mammals, zebrafish caspases are recruited to Asc speck (Kuri *et al.*, 2017). The
79 zebrafish genome encodes three inflammatory caspases which contain a PYD domain rather
80 than the CARD found in other vertebrates, to recruit the downstream, caspases, Caspa,
81 Caspb (Masumoto, Zhou, Felicia F. Chen, *et al.*, 2003) and casp19b (Spead *et al.*, 2018) to the
82 Asc speck. The functional homologues of mammalian caspase-1 in zebrafish, Caspa and
83 Caspb, are both able to induce cell death in zebrafish (Kuri *et al.*, 2017; Shkarina *et al.*, 2022),
84 and GSDMD cleavage and pyroptosis in human cells (Shkarina *et al.*, 2022). Caspb has been
85 shown to cleave the zebrafish Gasdermins, Gsdmea and Gsdmeb, in vitro (Chen *et al.*, 2021),
86 while caspa has been shown to co-localize with Asc-specks (Masumoto, Zhou, Felicia F Chen,
87 *et al.*, 2003; Kuri *et al.*, 2017)
88 Upon cleavage, GSDMs assemble into pores in the plasma membrane and lead to the release
89 of the cytosol including cytokines from the cell (Kayagaki *et al.*, 2015; Shi *et al.*, 2015; Liu *et*
90 *al.*, 2016; Sborgi *et al.*, 2016), a hallmark of pyroptotic cell death (Rühl and Broz, 2021). In
91 the absence of GSDM D, mammalian caspase-1 activates apoptosis as a default pathway
92 (Heilig *et al.*, 2020; Tsuchiya *et al.*, 2021), and the same was found for ASC-containing
93 inflammasomes in the absence of caspase-1 (Sagulenko *et al.*, 2013; Kitazawa *et al.*, 2017;
94 Lee *et al.*, 2018). Apoptosis is morphologically distinct from pyroptosis and characterized by
95 preservation of membrane integrity, characteristic membrane blebbing and progressive

fragmentation of the cell, in contrast to pyroptosis, which most commonly leads to a characteristic cell swelling.

We have previously developed optogenetic variants for human and zebrafish caspases which can be activated by light-induced oligomerization of Cry2olig, a photosensitive protein that undergoes rapid homo-oligomerization in response to blue light (Taslimi *et al.*, 2014; Shkarina *et al.*, 2022). This enabled us to selectively induce multiple forms of programmed cell death (PCD) in different cell types in vitro, organoids and in the live zebrafish larvae. We observed that zebrafish periderm cells are apically extruded from their surrounding epithelium upon stimulation of the inflammatory caspases but are basally extruded after activation of the apoptotic caspase-8 (Shkarina *et al.*, 2022).

To further study inflammasome formation and the resulting cell death in the zebrafish skin upstream of inflammatory caspases, we have now generated an optogenetic variant of zebrafish Asc (Opto-Asc), which efficiently induces speck formation in single cells in both layers of the larval skin. Opto-Asc specks cause inflammatory cell death followed by apical or basal extrusion in periderm cells, which is morphologically distinct from apoptosis. Asc-speck induced cell death is dependent on caspa and caspb but we could not confirm the role of gasdermins in this process, we therefore refrain from calling it pyroptosis. We show that Opto-Asc specks efficiently trigger cell death in the periderm via inflammatory apical or basal extrusion.

116 ## Results

117 **Optogenetic activation of Asc-oligomerization.**

118 The adaptor protein Asc is a core component of the canonical inflammasome and is well
119 conserved in vertebrates. Following interaction with the activated pattern recognition
120 receptors, it forms a large signaling complex (Asc speck) which recruits and activates
121 proinflammatory caspases. In the past, *in vivo* induction of inflammasome assembly has
122 been achieved only via overexpression of Asc or Nlrs (Kuri *et al.*, 2017), or by treatment with
123 proinflammatory chemicals like $CuSO_4$(Kuri *et al.*, 2017) or pathogens (Tyrkalska *et al.*, 2016;
124 Li *et al.*, 2018; Forn-Cuní, Meijer and Varela, 2019). However, chemical and bacterial
125 treatments affect the entire organism, which complicates targeted and controlled studies of
126 cellular and tissue response. In contrast, the over-expression of Asc efficiently triggers speck
127 formation and cell death, but does not allow targeting these processes in pre-determined
128 cells. To overcome these limitations and to enable specific induction of inflammasome
129 assembly with spatial and temporal control, we tagged zebrafish Asc with Cry2olig to
130 produce "Opto-Asc". Cry2olig is a protein module that, upon exposure to blue light,
131 reversibly oligomerizes within seconds (Taslimi *et al.*, 2014). We fused the mCherry-Cry2olig
132 domain to the N-terminal Pyd domain of Asc and placed this cassette under control of a heat
133 shock responsive element (HSE) (Bajoghli *et al.*, 2004), to be able to selectively induce
134 expression only in experimental larvae. We generated stable zebrafish lines for the plasmid
135 shown in Fig. 1A using Tol2-based random genome integration. The plasmid contains a
136 screening cassette in which tagRFP is expressed under the heart specific myosin light chain 2
137 promoter (cmlc2). Larvae were screened for red hearts at 2.5 days post fertilization (dpf).
138 Opto-Asc larvae were heat-shocked to induce expression and shielded from light to prevent
139 uncontrolled Opto-Asc activation. The photoactivation and imaging experiments were
140 performed at 3dpf as shown in Fig. 1B.

141 The expression of Opto-Asc became detectable around 3 h after the heat shock and reached
142 a maximum at around 12 h, leading to the mosaic expression of the Opto-Asc in single cells
143 of all tissues Skin cells of different layers can be identified by their distinct morphology:
144 periderm cells, the outer layer of skin cells, have sharp boundaries and a characteristic
145 pattern of actin ridges in the apical cortex. The underlying basal cells are smaller and have
146 less well-defined boundaries (Fig.1C). In absence of blue light stimulation, Opto-Asc did not

147 spontaneously form specks, but did so efficiently when stimulated with the 488 nm laser
148 (Fig. 1D).
149 The exposure of cells expressing Opto-Asc to 488nm laser light led to the formation of a
150 speck within minutes followed by immediate death of the cell in both epidermal layers (Fig.
151 1E). In the peridem cells were usually apically extruded from the within minutes after the
152 appearance of the speck. Even when small regions were selectively illuminated with the
153 488nm confocal laser, the specks also appeared in regions outside the illuminated area, and
154 sometimes even in the entire larva, likely due to the out-of-plane Cry2olig activation and
155 confocal light diffusion, and this could be avoided by using a 2-photon laser, in which case
156 which Opto-Asc oligomerization could be induced in single cells without affecting
157 surrounding cells (Fig.1F).
158 In muscle cells, illumination induced the formation of multiple stable oligomers of Opto-Asc
159 without inducing cell death (Supplementary Fig 1A), as also previously shown for Asc-
160 mKate2 specks (Kuri *et al.*, 2017). These Opto-Asc specks remained stable and did not
161 disperse after light exposure was terminated (for how long?). As control for the contribution
162 of the Asc moiety of the construct to oligomer formation we injected a mutant variant of
163 Cry2olig OptoR489E-Asc, which formed no oligomers at all and did not induce cell death
164 (Supplementary Figure 1B). Additionally, we also tested a C-terminal fusion of Cry2olig to
165 Asc, which also formed light-induced oligomers but did not trigger the formation of large
166 specks or cell death (data not shown). This indicated that the Asc moiety is not functional in
167 this fusion protein, suggesting that the functional induction of speck formation by Opto-Asc
168 in zebrafish requires oligomerization to be triggered close to the Pyd domains which have to
169 interact to form the initial filament (Dick *et al.*, 2016) or that zebrafish ASC requires some
170 post-translational modification that is hampered by the Cry2olig domain.
171 Kuri et al. showed that Asc specks could also be induced by overexpression of the Pyd-like
172 domain of one of the zebrafish NLR family members (si:dkeyp-4c4.1), most similar to
173 mammalian NLRP1. To induce speck formation upstream of Asc we generated optogenetic
174 variants of the full-length version as well as the Pyd domain of the NLR. However, the
175 expression of mCherry-Cy2olig-Nlr-FL, mCherry-Cry2olig-Nlr-Pyd or Nlr-Pyd-Cry2olig-
176 mCherry did not efficiently trigger speck formation in a time frame that was comparable to
177 Opto-Asc (data not shown).
178

179 **Optimization of heat shock and light exposure conditions for efficient Opto-Asc speck**
180 **induction**
181 During our initial experiments, we observed variability in the efficiency of speck formation
182 both between different larvae and between cells within a single larva. Thus, to identify
183 conditions for efficient induction of speck formation, we titrated both the heat shock
184 duration to maximize the expression of the construct and the laser illumination parameters
185 to optimize the light-induced oligomerization of Cry2olig.
186 To first determine the optimal heat shock parameters, we crossed the Opto-Asc line to a
187 Krt4:AKT-PH-GFP line, which enabled us to visualize the membrane outlines of skin cells in
188 order to count individual cells (Fig.2A). We then incubated the larvae at 39°C for different
189 periods of time and calculated the fraction of periderm cells expressing detectable levels of
190 Opto-Asc and the overall mean fluorescence intensity (MFI) of a defined region in each larva
191 (Fig.2C). While we found no significant correlation between the number of expressing cells
192 and overall MFI in any of the heat shock schemes (Fig.3D), we detected high expression
193 (>12.000 MFI) and a high percentage of expressing cells (>30 %) in those larvae that had
194 been heat-exposed for 35 min or longer. After longer heat shocks (40 min) the larvae started
195 to show deformations in their somites. We therefore performed all further experiments with
196 35 min heat shocks and, unless stated otherwise, used larvae expressing Opto-Asc in >30 %
197 of their cells for evaluation.
198 To next determine the effect of Opto-Asc expression levels on the efficiency of speck
199 formation, we exposed the heat-shocked larvae to 5% (1.24mWatt/µm2) 488 nm laser light
200 (an intensity normally used to image our GFP reporter lines). After 60 minutes, we counted
201 the percentage of Opto-Asc-positive epithelial cells in the imaged area and the percentage of
202 speck-forming cells among those Opto-Asc positive cells (Fig.2E). We found no correlation
203 between the number of positive cells and the likelihood of speck formation. However,
204 specks only ever formed in larvae in which more than at least 10 % of the cells were Opto-
205 Asc positive, indicating that there is a threshold for Opto-Asc expression below which cells
206 do not form a speck. Figure 2F shows three examples of larvae with different fractions of
207 Opto-Asc expressing cells which had been exposed to 5 % or 1 % 488 nm laser light. Larvae in
208 which few cells expressed Opto-Asc (here 12.5 % of cells) rarely formed specks, even after
209 long exposure times (1 stack/min for 60 min). Larvae with many expressing cells formed
210 specks within less than five minutes, regardless of laser power. In larvae with high Opto-Asc

211 levels, laser power as low as 0.1 % (0.025 mWatt/µm^2) was sufficient to induce speck
212 formation after several minutes (Fig. 2F).
213 We also observed an Opto-Asc expression level threshold for speck formation when
214 assessing individual cells. We measured the MFI of single cells in 14 larvae and scored for
215 each cell the time it took to form a speck under repeated blue light exposure for 60 minutes
216 (Fig.2G). While we found no absolute threshold for speck formation, 39.6 % of the cells with
217 Asc levels of >5000 MFI (relative units) formed specks within the period of observation,
218 usually within the first 30 min of exposure. Cells that did not form a speck within 60 min
219 (60.4 %) all had an MFI of < 5000 (relative units). When comparing cells only within
220 individual larvae, we similarly found that cells which did not form specks also had
221 significantly lower opto-Asc expression levels (Fig.2H). We also compared the effects of
222 constant illumination and a pulsed laser exposure, where a pulse is defined as the period of
223 imaging of a single stack (40 µm in 41 steps). We compared the effect of stimulation with
224 one and five pulses (Fig.2I) on the cells with the approximately similar opto-ASC expression
225 levels, which revealed that compared to constant light exposure (e.g. Fig.2H), fewer cells
226 formed a speck after pulsed illumination: 15,7% for five pulses (average MFI: 1999) and 17,7
227 % after one pulse (average MFI: 2063). The specking response to laser pulses was delayed,
228 sometimes up to 50 min (Fig.2J), similar to the dynamics we see at constant laser exposure
229 (cell death after up to 40 min post first illumination. While for most oligomerization
230 reactions, a single initial laser pulse was sufficient to trigger speck formation, a longer light
231 exposure increased the fraction of cells in which Cry2olig oligomerization was triggered
232 (Fig.2G).
233 Based on all of these observations, we chose the following conditions for our further
234 experiments: after 35 min HS we select larvae based on the percentage of expressing cells
235 (above 20%) and exposed them to 5% relative 488 nm laser intensity.
236
237 **Opto-Asc speck appearance and recruitment of endogenous Asc**
238 We have previously shown that specks induced by Asc-mKate2 efficiently recruited
239 endogenous Asc in the asc:asc-GFP line, where the open reading frame of endogenous Asc
240 was tagged with GFP (Kuri *et al.*, 2017). To test if Opto-Asc behaves in the same way as Asc-
241 mKate2, we assessed endogenous ASC and opto-ASC co-localization in single cells in larvae
242 expressing endogenous Asc (ubiquitous expression) and Opto-Asc (mosaic expression) using

243 Airyscan high resolution microscopy (Fig.3A). Endogenous Asc and Opto-Asc colocalized in
244 the cortical actin ridges, and during a speck formation they co-aggregated with the same
245 dynamics (Supplementary Fig. 2A and B). Like Asc-mKate, Opto-Asc was present throughout
246 the entire speck together with endogenous Asc (Supplementary Fig.2 C and D).
247 Opto-Asc specks were on average smaller than Asc-mKate2 specks (Supplementary Fig. 2E),
248 and unlike Asc-mKate2, Opto-Asc occasionally formed multiple specks which often
249 subsequently fused as the cell started to die. As an example of this, Fig.3B shows two
250 neighboring cells with similar Opto-Asc expression forming specks after light exposure. Both
251 cells recruited Asc to their membrane but while cell I formed a single speck, cell II formed
252 multiple irregularly shaped specks.
253
254 **Role of endogenous Asc and its domains in Opto-Asc-induced speck formation and cell**
255 **death**
256 All experiments reported so far were done in fish that had normal, endogenous Asc in
257 addition to the Opto-Asc. Since Opto-Asc recruites endogenous Asc, we do not know
258 whether cell death is triggered by endogenous or Opto-Asc. To test this, we used an Asc
259 loss-of-function mutant, $Asc^{\Delta 2/\Delta 2}$, in which the endogenous ASC has a CRISPR/Cas9 induced
260 frameshift mutation that introduces a premature stop codon p.Phe13*to create a protein-
261 null allele . To determine the ability of two different ASC domains, PYD and CARD, to induce
262 speck formation and cell death we egneratd Opto-PYD and Opto-CARD (both N-terminally
263 fused to mCherry-Cry2olig). We injected full-length Opto-Asc, Opto-Pyd and Opto-Card into
264 the $Asc^{\Delta 2/\Delta 2}$mutant line. We first tested the ability of Asc-mKate2 to function in this mutant
265 and found that it formed specks and induced cell death at the same level as in the wild-type
266 larvae, showing that Asc-mKate2 is fully functional and able to induce cell death (Fig. 4A).
267 In the wild-type Asc-GFP line, Opto-Asc, Opto-Pyd and Opto-Card induced speck formation
268 within five minutes, whereas showed a delayed speck formation (>2.5 min after first
269 aggregates were observed (N=3) The shrinking of the cell, which we consider an initial sign of
270 cell death upon opto-ASC activation, was seen as soon as the first oligomerization was
271 detectable for all of the constructs.
272 By contrast, in the $Asc^{\Delta 2/\Delta 2}$ knockout line, Opto-Asc, Opto-Pyd and Opto-Card formed
273 multiple smaller aggregates rather than a single large speck, indicating that endogenous Asc
274 may facilitate multiple Opto-Asc to coalesce to form a single speck structure. In this mutant,

275 Opto-Card did not induce cell death, consistent with the finding that inflammatory caspases
276 are recruited via the Pyd domain of Asc (Kuri *et al.*, 2017), and therefore, without
277 endogenous Asc, caspases could not be recruited to the Opto-Card construct. By contrast,
278 both Opto-Asc and Opto-PYD induced cell death, but often with a delay when compared to
279 Asc WT cells. (Fig. 4B).
280 When we measured the time between the first detectable oligomerization and first visible
281 signs of cell death, we found that in some $Asc^{\Delta 2/\Delta 2}$ knockout periderm cell death was
282 significantly delayed while in other $Asc^{\Delta 2/\Delta 2}$ and WT periderm the death was immediate after
283 the first oligomers were detected (Fig.4C).
284 These observations imply that the assembly of Asc into a clearly defined speck was not
285 required for downstream effectors to induce cell death. Figure 4D shows the example of
286 three cells expressing different levels of Opto-Pyd, which are normalized relative to the cell
287 with the weakest expression (1x). The cell with the highest level of Opto-Pyd (13.5x) entered
288 cell death before oligomerization was detectable, whereas in cells with intermediate (4.5x)
289 or low (1x) levels Opto-Pyd recruitment to the membrane and oligomerization significantly
290 preceded the appearance of first signs of cell death. This shows that the efficiency of cell
291 death induction is dependent on the amount of Opto-Asc or Opto-Pyd, and that in case of
292 high concentrations of Opto-Asc or Opto-Pyd, the formation of a visible speck is not required
293 for initiation of cell death.
294
295 **Cell extrusion after Opto-Asc speck formation**
296 Periderm cells typically respond to inflammasome formation by rapid cell death and apical
297 extrusion (Kuri *et al.*, 2017). Thus, we took advantage of opto-Asc-mediated inflammasome
298 formation to characterize the cellular events immediately following speck formation. Figure
299 5A shows an example of a cell that was extruded from the periderm -after speck formation.
300 The cell began to shrink within 30 sec of speck formation while the surrounding cells moved
301 in to fill the space. The dying cell lost its shape and started to form membrane blebs,
302 eventually swelled and was finally extruded from the cell layer. Once completely extruded,
303 the cell appeared round and lysed within minutes, as determined by the uptake of the
304 membrane-impermeable DNA-binding dye DRAQ7 which can only stain the cells following
305 membrane permeabilization (Fig. 5B). Most cells reached the lytic stage in 5-10 min post

306 illumination, although some remained fully extruded without lysing for up to 20 min post
307 speck formation (Fig. 5C).
308 Basal cells in the cell layer underlying the periderm also died following Opto-Asc speck
309 formation, but with a different morphology. They showed extensive fragmentations seen by
310 occurrence of membrane vesicles labeled by Akt-PH-GFP (Fig. 5D). The basal cells also
311 responded more slowly to speck formation than periderm cells and started to change
312 morphology only after ~5 minutes (Fig. 5E).
313
314 **Apical and basal cell extrusion in response to Opto-Asc specks**
315 The fate of the dying cells following Opto-Asc speck formation varied between cells within
316 and between different larvae. Some periderm cells were not extruded apically, as described
317 above, but instead left the periderm on the basal side. Another subset of cells fell in neither
318 of these groups; instead, part of their cell body was extruded apically, rounding up and
319 lysing, whereas another part was extruded basally, morphologically resembling the basally
320 extruded cells. As an example of this, Figure 6A shows cells located near each other in the
321 same larva, responding by apical extrusion (A), basal extrusion (B) or mixed extrusion (M).
322 To see if this variation in phenotype was determined by genetic differences in our fish lines
323 of mixed genetic background (Golden and AB2B2), we injected the Opto-Asc construct into
324 different commonly used laboratory strains (Fig. 6B). In most strains (AB, AB2B2 and Golden)
325 basal extrusion of periderm cells only occurred in a small number (<5 %) of cells per larva,
326 and not in all larvae. However, the WIK (Wild Indian karyotype) strain showed greater
327 variation, as did our experimental line (*Tg(Opto-asc)* x *Tg(Krt4:AKT-PH))* of mixed genetic
328 background (Opto-Asc: Golden and AB2B2, Krt4:AKT-PH: unknown). In these two lines,
329 considerably higher percentages of dying cells were basally extruded (38 % in WIK UPenn
330 and 64 % in *Tg(Opto-asc)*x *Tg(Krt4:AKT-PH)*).
331 To characterize the morphological differences between apical and basal cell extrusion, we
332 analyzed the dynamics of the actin cytoskeleton in the dying cells. We visualized actin with
333 an mNeonGreen (mNG)-tagged variant of the calponin homology domain of utrophin
334 (UtrCH) expressed under control of the UAS-promoter (*Tg(UAS:mNG-UtrCH*), which we
335 combined with a Krt4:Gal4 driver and UAS:lyn-tagRFP to label plasma membranes. Larvae
336 carrying these constructs showed stochastic expression of mNeonGreen-UtrCH in periderm
337 cells, which allowed us to follow actin dynamics in single cells. The overall response of the

338 actin cytoskeleton was similar in apically (Fig.6C) and basally (Fig. 6D) extruded cells. As the
339 cell started to shrink after speck formation, the actin ridges rapidly disappeared. Actin then
340 formed a diffuse ring at the periphery of the cell just prior to extrusion. The actin ring
341 contracted on the side of the cell that remained in contact with the epithelium. Basally
342 extruded cells were fragmented once fully internalized and were taken up by surrounding
343 cells or macrophages (Supplementary Fig. 3).
344 We previously showed that periderm cells dying by opto-zfCaspase-8-induced apoptosis
345 were also basally extruded from the periderm(Shkarina *et al.*, 2022). Thus, we analysed the
346 behaviour of their actin cytoskeleton in larvae derived from a cross of *Tg(Opto-caspase-8)*
347 with *Tg(Krt4:Gal4_ UAS:mNG-UtrCH-UAS:Lyn-tagRFP)* and found differences in the apical
348 actin ridges behavior. In contrast to the Opto-Asc-activated cells, apoptotic periderm cells
349 retained the original pattern of actin ridges while the cell was shrinking, with a proportional
350 scaling of the pattern until the cell was fully internalized (approximately 10 minutes) (Fig.6E).
351 While analyzing the behavior of the actin cytoskeleton in the cells surrounding dying cells
352 either after formation of an Asc speck or induction of apoptosis by Opto-Caspase-8, we
353 found that actin was always recruited to the membrane region that was in contact with the
354 dying cell, independent of the cell death phenotype (Supplementary Fig.4). We also analyzed
355 the actin cytoskeleton in basal cells dying in response to Asc-speck formation, which
356 revealed that while the cell was shrinking, its actin was re-localized to the membrane along
357 the borders to neighboring cells (Supplementary Fig. 5A) at the same time as those cells
358 started to migrate to close the gap created by the dying cell (Supplementary Fig. 5B).
359
360 **Role of caspases in Opto-Asc-induced apical extrusion**
361 Opto-ASC efficiently induced cell death in periderm and basal cells, but not in muscle cells
362 which the lack downstream effector caspases (Spead *et al.*, 2018). To test the role of
363 inflammatory caspases in speck-induced cell death, we disrupted the function of the two
364 caspase-1 homologues, caspa and caspb, by outcrossing *Tg(Opto-asc)* to an existing caspa
365 knock-out (KO) line (Kuri *et al.*, 2017), but unexpectedly saw no effect on extrusion of
366 periderm cells after Opto-Asc speck formation. We also used a CRISPR/Cas9 based method
367 to create F0 knock-out (Kroll *et al.*, 2021) as an alternative strategy of interfering with
368 caspase expression The synthetic short guide RNAs (sgRNAs) targeting different exons of
369 *caspa* and *caspb* (Fig. 7A) labeled in red in Fig. 7A were used in the double KO, and the ones

370 labelled in grey for single gene KOs. The efficiency of the knock-out was validated by
371 sequencing around all sgRNA binding sites.
372 Caspa deletion had no effect on the morphology or timing of Opto-Asc-induced cell death or
373 the extrusion efficiency (around 90 % of cells were still apically extruded). However,
374 periderm cells lacking Caspb were no longer extruded apically (Fig. 7B and C), but instead
375 they displayed the apoptotic phenotype, similar to the one observed in these cells after
376 Opto-Caspase-8 activation (Fig7D). In particular, these cells shrank while, retaining the
377 pattern of actin ridges (Fig.7E).
378 Thus, either caspa or caspb alone is sufficient to trigger cell death, but only caspb can trigger
379 apical extrusion.
380 In mammalian cells, inflammasome formation results in pyroptosis, which is defined as cell
381 death induced by Gasdermin pore formation (Liu *et al.*, 2016). The Zebrafish genome
382 encodes two gasdermins (Gsdms): GsdmEa and GsdmEb, which can be cleaved in vitro by
383 Caspb and apoptotic Caspase-8 and -3 respectively (Wang *et al.*, 2020; Chen *et al.*, 2021). To
384 test the role of these Gsdms in Opto-Asc-induced cell death and extrusion, we used two
385 ways of inactivating Gsdm function, a F0 CRISPR/Cas9 knock-out with four synthetic sgRNAs
386 for each gene, which has shown to induced >95% protein-null alleles (Kroll *et al.*, 2021)
387 and the Gsdm inhibitor LDC7559 similar as was used in (Isles *et al.*, 2021) to inhibit Gsdm
388 pores of neutrophils. However, neither of these treatments had an effect on the phenotype
389 or dynamics of cell death or on the polarity of extrusion (data not shown). We imaged and
390 genotyped at min 5 larvae for single and the double knockout of Gsdms.
391 We also measured the time span between speck formation and first signs of cell death, in
392 this case the start of cell deformation (shrinking) in different F0 KO backgrounds. F0 KO of
393 *caspb* led to a delay in the response to speck formation of up to 20 min, regardless of the
394 direction of extrusion (Fig. 7F). Double deletion of caspa and caspb delayed Opto-Asc-
395 induced cell death up to 180 min or longer. Similar to cells in which apoptosis was induced
396 by Opto-Caspase-8, these dying cells required a longer time (around 15 min) to be excluded
397 from the periderm than during Opto-Asc induced cell death in control larvae (Fig. 7G).
398 We also observed differences in the number and size of cell fragments, as measured by the
399 number and diameter of Akt-PH-GFP labeled membranes vesicles in basally extruded
400 peridermal cellsdepending on whether death was induced by Opto-Asc with or without
401 caspb or by Opto-Caspase-8 (Fig. 7H). Again, the phenotype of Opto-Asc-induced death in

402 the absence of caspb resembled that of Opto-Caspase-8-induced apoptosis. We will
403 therefore refer to this phenotype as opto-Asc-induced apoptosis.
404
405 **Ca^{2+} signaling in response to different types of cell death**
406 Pyroptotic cells have been shown to release ATP and other signaling molecules in order to
407 attract phagocytic cells (Wang *et al.*, 2013), in order to see if this affects Ca^{2+} signaling in
408 surrounding cells we looked at the Ca2+ signaling in the zebrafish skin in response to
409 necrosic cell death and apoptosis. We used the Ca^{2+} signaling reporter GCamp6 to
410 characterize the response of surrounding cells to cell death induced by Opto-Asc specks or
411 Opto-Caspase-8. We crossed the *Tg(Opto-asc)* line to *Tg(ß-actin:GCamp6)*, a line expressing
412 GCamp6 under the ubiquitously active ß-actin promoter(Chen, Xia, Michael R. Bruchas, *et*
413 *al.*, 2017) and subsequently imaged single cells expressing Opto-Asc and their immediate
414 surrounding at high temporal resolution (>5 sec frame rate).
415 Without induction of cell death, only sporadic and weak Ca^{2+} signals were seen in individual
416 cells at a frequency of about 0.2 per minute (3 cells in 15 min) within an imaging area of
417 around 24 cells corresponding to 13 mm^2 (Supplementary Fig.6A). In contrast, opto-ASC
418 activation induced strong Ca^{2+} responses in neighbors. As an example, Fig. 8A shows Ca^{2+}
419 signaling in periderm surrounding a cell being apically extruded following Opto-Asc speck
420 formation. The speck-forming cell as well as the basal cell underlying the site of the speck
421 showed increased Ca^{2+} levels within 15 sec of the speck becoming detectable; this preceded
422 the shrinking of the cell, which started after around 30 seconds. Ca^{2+} signaling then spread
423 to the surrounding cells in a wave-like manner. The first intense Ca^{2+} wave was immediately
424 followed by a smaller second wave, after which the signal became sporadic over the course
425 of 5 minutes and then subsided. Once the dying cell started blebbing, its internal Ca^{2+} level
426 remained high until lysis, indicating the loss of its ability to control intracellular Ca^{2+}
427 homeostasis.
428 To analyze these observations in a more quantitative manner, we used a two-dimensional
429 representation of time and space (derived from 3D kymographs; see supplementary Fig. 7)
430 to represent the calcium response in the area around the dying cell (Fig. 8B). The sum of the
431 signals along a radial sweep around the cell is represented on the y-axis (with the center of
432 the dying cell at y = 0) versus time on the x-axis (Supplementary Fig. 6B-D). The initial Ca^{2+}
433 waves (in cyan) appear as strong lines following the appearance of the speck (yellow arrow),

434 and the sporadic Ca^{2+} signals of surrounding cells appear as the weaker lines. The speck is
435 visible following its appearance as a magenta line, until it disappears following cell lysis. The
436 extruded cell appears as a cyan shadow once extruded, and remains visible until lysis.
437 Cells that were basally extruded responded to speck formation with immediate increased
438 Ca^{2+} levels in 3 out of 5 cases. For the first 15 minutes after the cell started to shrinkwe
439 detected on average 8.6 cases of increased Ca^{2+} signaling in basal cells and 30.7 in periderm
440 cells (N=3 cells of different larvae) (Supplementary Fig. 7A and B).
441 By contrast, caspase-8-induced apoptosis of periderm cells did not induce a comparable Ca^{2+}
442 wave in surrounding periderm (Fig. 8D), and apoptotic cells themselves never showed
443 increased Ca^{2+} levels. During the shrinking phase, before the cell was fully internalized, the
444 surrounding cells (mainly basal cells) showed only sporadic Ca^{2+} signaling. We detected on
445 average 21 cases of increased Ca^{2+} signaling in basal cells and 12.3 cases in periderm cells
446 directly adjacent to the dying cell within the first 15 minutes after the cell started to shrink
447 (N=3 cells of different larvae) (Supplementary Fig. 7C). Finally, when periderm cells died via
448 Asc-induced apoptosis in Caspb knock-outs, the Ca^{2+} response of surrounding cells and the
449 dying cell itself was similar to the response to Opto-Caspase-8-induction in the periderm.
450 In summary, the response of the surrounding cells depended on the direction of extrusion
451 and on the stimulus that triggered cell death. A strong calcium response in the form of a
452 wave in neighboring periderm cells and underlying basal cells occurred only in the case of
453 ASC-induced extrusion and most prominently when cells were apically extruded.
454
455

456 ## Discussion

457 Our results demonstrate that opto-ASc is an efficient tool to induce inflammasome
458 formation and ASC-dependent cell death in zebrafish. Compared to Asc over-expression
459 used in our earlier studies (Kuri *et al.*, 2017), or I infection models (Forn-Cuní, Meijer and
460 Varela, 2019), it allows a more precise spatial and temporal manipulation of inflammasome
461 activation and cell death. Heat-shock induced expression of Opto-Asc is highly variable
462 between cells within individual larvae and between larvae, which has both advantages and
463 disadvantages. Mosaically distinct Asc levels allow the assessment of the role of Asc levels
464 and the response of neighboring cells within the same experimental animal.
465 If a more uniform expression of Opto-Asc were desired, this could be achieved by the
466 expression of Opto-Asc under the control of tissue-specific promoters combined with Cre-
467 Lox or trans-activator-induced expression (Knopf *et al.*, 2010; Mosimann *et al.*, 2011; Gerety
468 *et al.*, 2013).
469 Opto-Asc oligomerization is efficiently induced within minutes by constant exposure to 488
470 nm light. After a single light pulse, specks were often not observed immediately, but
471 appeared with a delay of up to 40 min. This is unexpected, because it is unlikely that Cry2-
472 olig would remain active for so long that dimerization could be delayed for more than a few
473 minutes (Taslimi *et al.*, 2014), and one would expect that even a single initial dimerization of
474 Opto-Asc would have led to the immediate recruitment of the endogenous Asc that is
475 available throughout the cell. Our observations may suggest that the initial seeding event
476 could have created a dimer that was not yet active, but that a second step of maturation
477 could subsequently occur. This highlights the fact that we still know very little about the
478 unusual dynamics of speck assembly, or the mystery why the cell normally always forms only
479 one single speck.
480 In response to the formation of an Opto-Asc speck periderm cells died in two
481 morphologically different ways. Cells were extruded either apically or basally, and some cells
482 were simultaneously extruded in both ways. Apical extrusion of periderm cells has been
483 described not only in response to infection, but also in response to treatment with the
484 antibiotic geneticin (G418) (Eisenhoffer and Rosenblatt, 2011) and during tissue
485 homeostasis as a response to cell crowding (Eisenhoffer *et al.*, 2012). Apoptotic stimuli like
486 geneticin have been shown to induce extrusion via sphingosine-1 phosphate (S1P) and its
487 receptor, which is expressed in the surrounding cells. We have previously shown that S1P

488 signaling does not seem to drive extrusion of pyroptotic cells in Caco-2 cell co-cultures
489 (Shkarina *et al.*, 2022), but so far it is unclear if S1P signaling or another mechanism
490 activated downstream of the inflammasome is responsible for apical extrusion. Although the
491 factors determining the direction of extrusion remain to be discovered, the different ratios
492 of apical and basal extrusion of periderm cells in different zebrafish strains suggest a genetic
493 component.
494 These findings indicate that different types of cell death are not entirely separable, but that
495 they represent different manifestations of parallel and interconnected signaling pathways,
496 the overall balance of which defines the final outcomes. This is also evident from other
497 studies in the past, where disrupting one pathway directs the cell towards a different
498 pathway that may have a different phenotypic outcome (Tsuchiya *et al.*, 2019). Perhaps it is
499 only through experimental activation of the most downstream effector that a 'pure'
500 phenotype can be induced.
501 In the case of zebrafish periderm, we identified Caspb as essential for apical extrusion. In the
502 absence of caspb, cells die with an apoptotic morphology in response to speck formation .
503 The requirement for caspb for apical extrusion and lysis might also explain the difference in
504 the response to Asc-speck formation between the periderm and the underlying basal cells.
505 According to cell type specific RNA sequencing data (Cokus *et al.*, 2019), basal cells express
506 ten times lower levels of Caspb than periderm cells.
507 Although Caspa localizes to the Asc speck (Kuri *et al.*, 2017) and is necessary for rapid cell
508 death if no Caspb is present, we did not find it to be necessary for speck induced extrusion.
509 This contradicts our own previous work, in which we identified caspa as responsible for fast
510 extrusion after speck formation (Kuri *et al.*, 2017) . We have now re-analyzed our previous
511 data (Supplementary figure 8) and found that the delay between speck formation and cell
512 death can be partially explained by the type of cell that was imaged, namely basal cells
513 although we could observe a much stronger delay between speck formation and cell death
514 compared to WT basal cells.
515 Zebrafish Caspa and Caspb are thus redundant in their role as rapid cell death inducers, but
516 the downstream mechanisms that lead to either extrusion or apoptosis of periderm cells are
517 yet to be identified.
518 Apoptosis and Asc-induced cell death are both initiated within a short time after speck
519 formation and cause the recruitment of actin in surrounding cells to the side facing the dying

520 cells. The closure of the surrounding epithelium above or below the extruded cell is faster
521 for Asc-induced extrusion than for apoptosis. This difference in rate of wound closure could
522 be caused by different dynamics in the cell itself, or in the surrounding cells. The fact that we
523 observe an immediate Ca^{2+} response in the case of Asc-induced death, but not apoptosis,
524 indicates signalling from the dying cell to the surrounding epithelium, and this signal differs
525 between cells dying apoptotically or by Asc-induced death The dependence on the fast
526 apical extrusion and the rapid Ca^{2+} response require Caspb, pointing to a Caspb-dependent
527 signalling event. A similar reaction was observed in cultured intestinal epithelial cells in
528 which a bacterial infection sensed by the NAIP/NLRC4 inflammasome induce a fast myosin-
529 dependent contraction in surrounding cells. This reaction was dependent on the activation
530 of sub-lytic GSDMD pores and the resulting ion flux and independent of the cell death or
531 extrusion of the cell (Ventayol et al., 2021).
532 Zebrafish do not have a direct homolog of GsdmD but two homologues of GsdmE
533 (Gsdmea/b). Human GsdmE was shown to be activated downstream of caspase-3 during
534 apoptosis (Wang *et al.*, 2017) and it plays a role in the caspase-3 mediated lytic death of
535 primary human keratinocytes after viral inactivation of the Bcl-2 pathway (Orzalli *et al.*,
536 2021). Both zebrafish gasdermins can be cleaved by caspb and other apoptotic caspases (but
537 not caspa) *in vitro* (Chen *et al.*, 2021) .It was therefore surprising to find that we did not see
538 a change in peridermal keratinocyte cell death after ASC-speck formation when we knocked
539 out Gsdme a and b by CRISPR/Cas9, or treated fish with a Gasdermin inhibitor. Although our
540 CRISPR/Cas 9 strategy is highly efficient for other genes, we cannot rule out that Gsdme a
541 and b are redundant in their function to mediate Caspb dependent extrusion and that a
542 relatively small amount is sufficient to induce this form of cell death. Additionally, we find
543 that cells which are extruded do not lyse immediately upon swelling which is normally the
544 case in pyroptotic cultured cells (Shkarina *et al.*, 2022). Since we find a caspb-dependent
545 difference in cell death phenotypes, the question arises which other component could cause
546 the apical extrusion of cells and wave-like Ca^{2+} signaling response in surrounding cells.
547 Possible candidates could be pannexins, especially pannexin1a which is expressed in skin
548 cells (Cokus *et al.*, 2019) and is necessary downstream of Caspase-11 to induced pyroptosis
549 in response to LPS in mouse macrophages (Yang *et al.*, 2015). The release of ATP caused by
550 pannexin pores might explain the strong calcium wave in caspb-dependent extrusion of
551 peridermal keratinocytes (Mori *et al.*, 2022) .

552 # Materials and Methods

553 ## Zebrafish husbandry, transgenic lines, and genotyping

554 Zebrafish (*Danio rerio*) were cared for using standard procedures as described previously
555 (Westerfield, 2000) and in accordance with EMBL guidelines. All experimental procedures
556 were approved by the EMBL Institutional Animal Care and Use Committee (IACUC nos. 2019-
557 03-19ML). We used the following zebrafish wildtype lab strains: AB2B2, AB, golden and Wild
558 Indian Karyotype (WIK). The *Tg(HSE:mCherry-Cry2olig-asc)* line was generated by co-
559 injecting embryos at the one-cell stage with Opto-caspase plasmids with transposase mRNA
560 (100 ng/µl). To follow the actin dynamics in skin cells, we used the *Tg(krt4:Gal4) line* (Wada
561 *et al.*, 2013) crossed to *Tg(6xUAS:mNeonGreen-UtrCH_6xUAS:lyn-tagRFP)* generated in
562 the lab of D.Gilmour by Jonas Hartmann. Actin dynamics in basal skin cells were visualized in
563 the *Tg(rcn3:Gal4*) line (Ellis, Bagwell and Bagnat, 2013) crossed to *Tg(6xUAS:mNeonGreen-*
564 *UtrCH_6xUAS:lyn-tagRFP)*. To induce specks and follow endogenous ASC we used
565 *Tg(HSE:asc-mKate2)* and the endogenously tagged asc:asc-GFP line (Kuri *et al.*, 2017). To
566 induce apoptotic cell death, we used *Tg(HSE:mCherry-Cry2olig-caspase-8)* (Shkarina *et al.*,
567 2022). For monitoring Ca^{2+} signaling we used *Tg(ß-actin:GCamp6)* (Chen, Xia, Michael R
568 Bruchas, *et al.*, 2017).
569

570 ## Cloning of Opto-Asc and Opto-Nlr variant constructs and transient expression

571 The Cry2olig-mCherry construct (plasmid #60032) was obtained from Addgene, and
572 plasmids containing Asc, Asc(4xmut), Pyd, Nlr and Card published in (Kuri *et al.*, 2017) were
573 used as cloning templates. The initial HSE:mCherry-Cy2olig ASC construct was cloned as
574 described in (Shkarina *et al.*, 2022). Other constructs containing ASC variants (PYD and
575 CARD) used the HSE:mCherry-Cy2olig-Asc as background and were modified by seamless
576 cloning using the NEB Assembly Kit, after SmaI/EcoRV or XmaI/EcoRV digestion of the
577 plasmid (replacing Asc). The following constructs were generated and used for transient
578 expression: HSE:mCherry-Cry2oligR489E, HSE:mCherry-Cry2olig-Pyd, HSE:mCherry-Cry2olig-
579 Card, HSE:mCherry-Cry2olig-Nlr-FL , HSE:mCherry-Cry2olig-Nlr-Pyd. All inserts were verified
580 by sequencing, and constructs are deposited in the European Plasmid Repository
581 (https://www.plasmids.eu)For expression of transient constructs, we co-injected expression
582 plasmids with Tol2 transposase mRNA (100 ng/µl) in embryos at the one-cell stage.

583 Larvae were screened at 2.5 dpf for expression of tag:RFP in the heart as described in (Kuri
584 *et al.*, 2017); For heat-shock driven expression, we incubated larvae at 2.5-3 dpf in 2 ml
585 tubes in a heating block at 39°C.
586

587 ## CRISPR/Cas9-mediated asc zebrafish knockout

588 We deisgned a custom gBLOCK (Integrated DNA Technologies) incorporating a guide RNA-
589 targeting sequence preceded by a T7 promoter sequence. Guide RNAs against exon 1 of *asc*
590 were used with the following sequences: 5'-GGTGGAGATCGAAGATCAAG-3' and 5'-
591 GCAGCTGCAGGAGGCTTTTG-3' respectively. Guide RNAs were synthesized using MEGA
592 shortscriptTM Kit (Applied Biosystems), according to the manufacturer's protocol, and were
593 purified using RNeasy Mini Kit (Qiagen, #74106). Cas9 mRNA was synthesized using
594 mMESSAGE mMACHINE® SP6 Transcription Kit (Thermo Fisher Scientific, #AM1340). 2 nL of
595 a mixture containing 250 ng/µL gRNA and 0.1 mg/mL Cas9 protein was injected into the yolk
596 of 1-cell AB zebrafish embryos.
597 Genotyping was performed by extracting genomic DNA from fin clips or larvae using the
598 QuickExtract DNA extraction solution (Epicentre) and amplifying loci using EMBL in-house
599 Phusion polymerase, primers are listed in Supplementary Table 1.
600

601 ## F0 CRISPR Screen

602 The F0 CRISPR screen was performed as described in (Kroll *et al.*, 2021) for caspa, caspb,
603 *gsdmea*, *gsdmeb* and *caspase-8a*. sgRNA target sites were selected for high predicted
604 cleavage efficiency within various exons of candidate genes using CCTop (Stemmer *et al.*,
605 2015).
606 Sequences of synthetic sgRNAs and gene identifiers are listed in Supplementary Table 1. We
607 used 3-4 synthetic sgRNAs (Sigma) per gene, which were diluted in water to a concentration
608 of 100 µM. Cas9 protein was produced by the EMBL PEPCore facility and stored in a
609 concentration of 62,5 µM in Cas9 buffer (20 mM Tris-HCl, 500 mM KCl and 20 % vol glycerol).
610 For each experiment, we freshly mixed equal volumes of sgRNA and protein solution (1 µl
611 sgRNA per 1 µl Cas9) and injected the mixture into early embryos within the first 15 min
612 after fertilization. All CRISPR KOs were confirmed by PCR and sequencing around target
613 sites.
614

615 ## Live imaging and optogenetics

616 Zebrafish larvae were anaesthetized using 4mg/ml tricaine pH 7 and mounted on their right
617 side in 0.75% low melting agarose on MaTec glass bottom petri dishes (35mmNo. 1.5
618 coverglass, 0.16-0.19 mm). Live imaging was performed at 20°C using a Zeiss LSM780 NLO
619 confocal microscope (Carl Zeiss) and a 40× C-Apochromat (NA 1.20) water immersion
620 objective (Carl Zeiss). To image GFP, mNeonGreen and the GCamp6 Ca^{2+} reporter, we used
621 the 488 nm multiline Argon laser (Lasos Laser GmbH). To image mCherry and lyn-tagRFP, we
622 used a HeNe laser at 561 nm. For detection of the far-red dye DRAQ7 we used the HeNe 681
623 laser.
624 We determined the laser intensity for the 488 nm laser at regular intervals using a chroma
625 slide at a fixed laser power of 5 %. The total laser power was measured using a laser power
626 meter (THORLABS GmbH Dachau Germany SN: P0023941) equipped with the sensor S121C
627 400-1100nm with a capability of measuring 500mW. Whenever not stated otherwise, we
628 used 5 % 488 argon laser power (24.8microWatt/pixel) to stimulate oligomerization of
629 optogenetic constructs.
630 For 2-photon activation of Opto-ASC in single cells, we used a 140-fs pulsed multi photon
631 laser (chameleon; Coherent) of the LSM780 NLO and operated the microscope using the Zen
632 Black Software (Carl Zeiss, 2012 version) together with the Pipeline Constructor Macro (Politi
633 et al., 2018).
634 For overnight imaging of whole larvae, we used a 20x air objective (Carl Zeiss) and acquired
635 multiple stacks (2x7) to cover the entire larva. Stacks were then stitched together using the
636 Zen Black software. Stacks were acquired every 15 minutes for 12-16 hrs.
637 For high-resolution time-lapse imaging of the Opto-ASC speck, Opto-PYD and Opto-CARD we
638 used a Zeiss 880 Airyscan and imaged in Airy fast mode with a C-apochromat 40x/1.2W Korr
639 FCS M27 objective. For activation of opto-constructs and detection of GFP we used 0.2%
640 488nm and for detection of mCherry 1.5% 561nm. To detect the GCamp6 signal, we
641 optimized imaging conditions to reach a frame rate below 5 sec. The stack size was 8 µm (1
642 µm z resolution).
643

644 ## Image analysis and quantification

645 We used Fiji ImageJ for image analysis (Schindelin *et al.*, 2012). Images acquired on the Zeiss
646 880 Airyscan were processed with Zen black software (Zeiss). We used the cell counter

647 plugin to manually count total numbers of periderm cells and numbers of periderm cells
648 expressing Opto-Asc. Example images are always presented as maximum intensity z-
649 projections. The total mean fluorescence of larvae was measured in maximum z-projections
650 in the region of interest (ROI) manually defined by the outline of the larva. To determine the
651 expression of Opto-Asc in single cells, we chose the three z-planes in which most of the cell
652 was visible and measured MFI in a selected region with uniform expression in an average
653 intensity z-projection.
654 Line profiles for high resolution images of specks were normalized by dividing by the average
655 gray value and subtraction of the lowest gray value. For measuring speck size, a line was
656 drawn through the longest diameter of the speck; the diameter was determined by
657 measuring the distance between the two points of maximum slope of the plot profile along
658 the line.
659 To determine the growth of specks, we marked the outlines of the speck in each time frame
660 for Opto-Asc and asc-GFP separately and measured the area. We started the measurements
661 at the first time point where mCherry/GFP visibly aggregated. We calculated the time
662 difference starting from the appearance of the first mCherry/mKate2 aggregates to the time
663 point where total intensity (intensity * area) of the speck reached a constant value.
664 To determine if a periderm cell was extruded apical, basal or in both directions we used the
665 bright field imaging, anything that is retained below the periderm was consider as basally
666 extruded, everything that left the tissue and dissociated from the epithelial layer to the
667 water was considered apically extruded. In case of mixed extrusion part of the cell was
668 retained the other part apically extruded.
669 For estimating the time between speck formation and initiation of cell death, we calculated
670 the interval from first detectable Opto-Asc aggregates to the time when the cell outline first
671 deformed. For the analysis of Ca^{2+} signaling of bystander cells in response to cell death, we
672 generated Kymographs for a circular area around the dying cells using the Radial Reslice Fiji
673 plugin (Cooper, 2009) which measures the pixel intensity along a line rotating around a
674 center in 360 degree. By creating an average projection of all lines, we created a two-
675 dimensional representation of the area around the cell for every time point. The exact
676 procedure with examples images is shown in Supplementary Fig. 6.

677 To quantify the Ca^{2+} response of bystander cells to basal extrusion and apoptosis, we
678 manually counted the number of periderm cells and basal cells which showed a GCamp6
679 signal for every minute after initiation of cell death for 15 min.
680

681 ## Statistics

682 All statistical analysis was done using Prism (version 9) (Graphpad). P-value ranges are
683 included in figures as follows: * is $p<0.05$, ** is $p<0.01$ *** is $p<0.001$ and **** is $p<0.0001$.
684 For comparison of different heat shock conditions (Fig. 2B and C) and the comparisons in Fig.
685 7F-H, we used ordinary one-way ANOVA. For determining correlations, we used simple
686 linear regression. To compare average MFI between speck forming and non-speck forming
687 cells, we used a Wilkoxon Test. To compare sizes of specks and time of speck formation, we
688 used a Mann-Wittney test. For the difference in time shown in Fig. 4C and Fig. 5E, we
689 assumed unequal standard deviations and used a t-test with Welch's correction.
690

691 ## Chemical treatments

692 For the detection of cell lysis, we used Draq7 (Invitrogen), a far-red dye that only stains
693 nuclear DNA once the membrane integrity is lost. We preincubated fish in 0.3 µM (1:1000)
694 Draq7 in E3 fish medium for 1 hr and added the dye directly to the low-melting agarose and
695 the fish medium in which larvae were imaged, to a concentration of 0.3. µM.
696 To inhibit gasdermin pore formation, we treated 2dpf larvae over night with 10 µM to 100
697 µM Gasdermin D inhibitor LDC7559 (MedChemExpress). The inhibitor was added directly to
698 the fish water as described in (Isles *et al.*, 2021), and larva were imaged at 3 dpf.
699

700 ## Acknowledgements:

701 The authors thank the Advanced Light Microscopy Facility (AMLF) at the EMBL-Heidelberg
702 for their continued support and Manuel Gunkel for his help with laser intensity
703 measurements. The authors thank Darren Gilmour and Jonas Hartmann for providing the
704 *Tg(6xUAS:mneonGreen-UtrCH)* zebrafish line. We thank Alexandre Paix for providing
705 guidance and material for CRISPR/Cas9 experiments and Takehito Tomita for help with
706 analysis of GCamp6 imaging data.
707

Author's contribution:

Author contributions: EH and ML conceptualized the study. KS and PB designed and created initial optogenetic tools. EH designed in vivo experiments. EH and SD performed in vivo experiments. BR and JRX created the Asc (Pycard) knockout fishline. All authors contributed to data analysis and manuscript writing.

715 Literature

716 Bajoghli, B. *et al.* (2004) 'An artificial promoter construct for heat-inducible misexpression
717 during fish embryogenesis.', *Developmental biology*, 271(2), pp. 416–30. doi:
718 10.1016/j.ydbio.2004.04.006.
719 Chan, K. Y. *et al.* (2022) 'Skin cells undergo asynthetic fission to expand body surfaces in
720 zebrafish', *Nature*. Springer US, 605(7908), pp. 119–125. doi: 10.1038/s41586-022-04641-0.
721 Chen, H. *et al.* (2021) 'Zebrafish gasdermin E cleavage-engaged pyroptosis by inflammatory
722 and apoptotic caspases', *Developmental and Comparative Immunology*. Elsevier Ltd,
723 124(July), p. 104203. doi: 10.1016/j.dci.2021.104203.
724 Chen, J., Xia, L., Bruchas, Michael R, *et al.* (2017) 'Imaging early embryonic calcium activity
725 with GCaMP6s transgenic zebra fi sh', *Developmental Biology*. Elsevier Inc., 430(2), pp. 385–
726 396. doi: 10.1016/j.ydbio.2017.03.010.
727 Chen, J., Xia, L., Bruchas, Michael R., *et al.* (2017) 'Imaging early embryonic calcium activity
728 with GCaMP6s transgenic zebrafish', *Developmental Biology*. Elsevier Inc., 430(2), pp. 385–
729 396. doi: 10.1016/j.ydbio.2017.03.010.
730 Churchill, M. J., Mitchell, P. S. and Rauch, I. (2022) 'Epithelial Pyroptosis in Host Defense',
731 *Journal of Molecular Biology*. Elsevier Ltd, 434(4), p. 167278. doi:
732 10.1016/j.jmb.2021.167278.
733 Cokus, S. J. *et al.* (2019) 'Tissue-specific transcriptomes reveal gene expression trajectories in
734 two maturing skin epithelial layers in zebrafish embryos', *G3: Genes, Genomes, Genetics*,
735 9(10), pp. 3439–3452. doi: 10.1534/g3.119.400402.
736 Cooper, J. (2009) 'Radial Reslice plugin'. Available at: Radial_Reslice.java.
737 Dick, M. S. *et al.* (2016) 'ASC filament formation serves as a signal amplification mechanism
738 for inflammasomes', *Nature Communications*, 7(May). doi: 10.1038/ncomms11929.
739 Eisenhoffer, G. T. *et al.* (2012) 'Crowding induces live cell extrusion to maintain homeostatic
740 cell numbers in epithelia', *Nature*. Nature Publishing Group, 484(7395), pp. 546–549. doi:
741 10.1038/nature10999.
742 Eisenhoffer, G. T. and Rosenblatt, J. (2011) 'Live imaging of cell extrusion from the epidermis
743 of developing zebrafish', *Journal of Visualized Experiments*, d(52), pp. 2–5. doi:
744 10.3791/2689.
745 Ellis, K., Bagwell, J. and Bagnat, M. (2013) 'Notochord vacuoles are lysosome-related
746 organelles that function in axis and spine morphogenesis', *Journal of Cell Biology*, 200(5), pp.

747 667–679. doi: 10.1083/jcb.201212095.
748 Evavold, C. L. *et al.* (2018) 'The Pore-Forming Protein Gasdermin D Regulates Interleukin-1
749 Secretion from Living Macrophages', *Immunity*. Elsevier Inc., 48(1), pp. 35-44.e6. doi:
750 10.1016/j.immuni.2017.11.013.
751 Forn-Cuní, G., Meijer, A. H. and Varela, M. (2019) 'Zebrafish in inflammasome research',
752 *Cells*, 8(8), pp. 1–14. doi: 10.3390/cells8080901.
753 Gerety, S. S. *et al.* (2013) 'An inducible transgene expression system for zebrafish and chick',
754 *Development (Cambridge)*, 140(10), pp. 2235–2243. doi: 10.1242/dev.091520.
755 Heilig, R. *et al.* (2018) 'The Gasdermin-D pore acts as a conduit for IL-1β secretion in mice',
756 *European Journal of Immunology*, 48(4), pp. 584–592. doi: 10.1002/eji.201747404.
757 Heilig, R. *et al.* (2020) 'Caspase-1 cleaves Bid to release mitochondrial SMAC and drive
758 secondary necrosis in the absence of GSDMD', *Life Science Alliance*, 3(4), pp. 1–15. doi:
759 10.26508/LSA.202000735.
760 Howe, K. *et al.* (2016) 'Structure and evolutionary history of a large family of NLR proteins in
761 the zebrafish.', *Open biology*, 6(4), p. 160009. doi: 10.1098/rsob.160009.
762 Isles, H. M. *et al.* (2021) 'Pioneer neutrophils release chromatin within in vivo swarms', *eLife*.
763 eLife Sciences Publications Ltd, 10. doi: 10.7554/eLife.68755.
764 Kayagaki, N. *et al.* (2015) 'Caspase-11 cleaves gasdermin D for non-canonical inflammasome
765 signalling', *Nature*, 526(7575), pp. 666–671. doi: 10.1038/nature15541.
766 Kitazawa, M. *et al.* (2017) 'ASC Induces apoptosis via activation of caspase-9 by enhancing
767 gap junction-mediated intercellular communication', *PLoS ONE*. Public Library of Science,
768 12(1). doi: 10.1371/journal.pone.0169340.
769 Knopf, F. *et al.* (2010) 'Dually inducible TetON systems for tissue-specific conditional gene
770 expression in zebrafish.', *Proceedings of the National Academy of Sciences of the United*
771 *States of America*, 107(46), pp. 19933–8. doi: 10.1073/pnas.1007799107.
772 Kroll, F. *et al.* (2021) *A simple and effective f0 knockout method for rapid screening of*
773 *behaviour and other complex phenotypes*, *eLife*. doi: 10.7554/eLife.59683.
774 Kuri, P. *et al.* (2017) 'Dynamics of ASC speck formation during skin inflammatory responses in
775 vivo'. doi: 10.1101/111542.
776 Lee, B. L. *et al.* (2018) 'ASC- A nd caspase-8-dependent apoptotic pathway diverges from the
777 NLRC4 inflammasome in macrophages', *Scientific Reports*. Nature Publishing Group, 8(1).
778 doi: 10.1038/s41598-018-21998-3.

779 Lee, R. T. H., Asharani, P. V. and Carney, T. J. (2014) 'Basal keratinocytes contribute to all
780 strata of the adult zebrafish epidermis', *PLoS ONE*, 9(1). doi: 10.1371/journal.pone.0084858.
781 Li, J. *et al.* (2018) 'Characterization of an NLRP1 Inflammasome from Zebrafish Reveals a
782 Unique Sequential Activation Mechanism Underlying Inflammatory Caspases in Ancient
783 Vertebrates', *The Journal of Immunology*, p. ji1800498. doi: 10.4049/jimmunol.1800498.
784 Liu, X. *et al.* (2016) 'Inflammasome-activated gasdermin D causes pyroptosis by forming
785 membrane pores.', *Nature*. Nature Publishing Group, 535(7610), pp. 153–158. doi:
786 10.1038/nature18629.
787 Martinon, F., Burns, K. and Tschopp, J. (2002) 'The Inflammasome: A molecular platform
788 triggering activation of inflammatory caspases and processing of proIL-β', *Molecular Cell*,
789 10(2), pp. 417–426. doi: 10.1016/S1097-2765(02)00599-3.
790 Masumoto, J., Zhou, W., Chen, Felicia F., *et al.* (2003) 'Caspy, a zebrafish caspase, activated
791 by ASC oligomerization is required for pharyngeal arch development', *Journal of Biological*
792 *Chemistry*, 278(6), pp. 4268–4276. doi: 10.1074/jbc.M203944200.
793 Masumoto, J., Zhou, W., Chen, Felicia F, *et al.* (2003) 'Caspy , a Zebrafish Caspase , Activated
794 by ASC Oligomerization Is Required for Pharyngeal Arch Development *', 278(6), pp. 4268–
795 4276. doi: 10.1074/jbc.M203944200.
796 Mori, Y. *et al.* (2022) 'Extracellular ATP facilitates cell extrusion from epithelial layers
797 mediated by cell competition or apoptosis', *Current Biology*. Elsevier Inc., 32(10), pp. 2144-
798 2159.e5. doi: 10.1016/j.cub.2022.03.057.
799 Mosimann, C. *et al.* (2011) 'Ubiquitous transgene expression and Cre-based recombination
800 driven by the ubiquitin promoter in zebrafish', *Development (Cambridge, England)*, 138(1),
801 pp. 169–177. doi: 10.1242/dev.059345.
802 Novoa, B. and Figueras, A. (2012) 'Zebrafish: Model for the Study of Inflammation and the
803 Innate Immune Response to Infectious Diseases', in Lambris, J. D. and Hajishengallis, G. (eds)
804 *Current Topics in Innate Immunity II*. New York, NY: Springer New York, pp. 253–275. doi:
805 10.1007/978-1-4614-0106-3_15.
806 Orzalli, M. H. *et al.* (2021) 'Virus-mediated inactivation of anti-apoptotic Bcl-2 family
807 members promotes Gasdermin-E-dependent pyroptosis in barrier epithelial cells', *Immunity*.
808 Elsevier Inc., 54(7), pp. 1447-1462.e5. doi: 10.1016/j.immuni.2021.04.012.
809 Renshaw, S. A. and Trede, N. S. (2012) 'A model 450 million years in the making: Zebrafish
810 and vertebrate immunity', *DMM Disease Models and Mechanisms*, 5(1), pp. 38–47. doi:

811 10.1242/dmm.007138.
812 Rühl, S. and Broz, P. (2021) 'Regulation of Lytic and Non-Lytic Functions of Gasdermin Pores',
813 *Journal of Molecular Biology*, 434(4). doi: 10.1016/j.jmb.2021.167246.
814 Sagulenko, V. *et al.* (2013) 'AIM2 and NLRP3 inflammasomes activate both apoptotic and
815 pyroptotic death pathways via ASC', *Cell Death and Differentiation*, 20(9), pp. 1149–1160.
816 doi: 10.1038/cdd.2013.37.
817 Santana, P. T. *et al.* (2016) 'Is the inflammasome relevant for epithelial cell function?',
818 *Microbes and Infection*, 18(2), pp. 93–101. doi:
819 https://doi.org/10.1016/j.micinf.2015.10.007.
820 Sborgi, L. *et al.* (2016) ' GSDMD membrane pore formation constitutes the mechanism of
821 pyroptotic cell death ', *The EMBO Journal*, 35(16), pp. 1766–1778. doi:
822 10.15252/embj.201694696.
823 Schindelin, J. *et al.* (2012) 'Fiji: An open-source platform for biological-image analysis',
824 *Nature Methods*, 9(7), pp. 676–682. doi: 10.1038/nmeth.2019.
825 Shi, J. *et al.* (2015) 'Cleavage of GSDMD by inflammatory caspases determines pyroptotic cell
826 death', *Nature*, 526(7575), pp. 660–665. doi: 10.1038/nature15514.
827 Shkarina, K. *et al.* (2022) 'Optogenetic activators of apoptosis , necroptosis , and pyroptosis',
828 221(6).
829 Spead, O. *et al.* (2018) 'Characterization of the caspase family in zebrafish', *PLoS ONE*, 13(5).
830 doi: 10.1371/journal.pone.0197966.
831 Stein, C. *et al.* (2007) 'Conservation and divergence of gene families encoding components of
832 innate immune response systems in zebrafish', 8(11). doi: 10.1186/gb-2007-8-11-r251.
833 Stemmer, M. *et al.* (2015) 'CCTop: An intuitive, flexible and reliable CRISPR/Cas9 target
834 prediction tool', *PLoS ONE*, 10(4). doi: 10.1371/journal.pone.0124633.
835 Taslimi, A. *et al.* (2014) 'An optimized optogenetic clustering tool for probing protein
836 interaction and function', *Nature Communications*. Nature Publishing Group, 5. doi:
837 10.1038/ncomms5925.
838 Tsuchiya, K. *et al.* (2019) 'Caspase-1 initiates apoptosis in the absence of gasdermin D',
839 *Nature Communications*. Springer US, 10(1). doi: 10.1038/s41467-019-09753-2.
840 Tsuchiya, K. *et al.* (2021) 'Gasdermin D mediates the maturation and release of IL-1α
841 downstream of inflammasomes', *Cell Reports*. ElsevierCompany., 34(12), p. 108887. doi:
842 10.1016/j.celrep.2021.108887.

843 Tweedell, R. E., Malireddi, R. K. S. and Kanneganti, T. D. (2020) 'A comprehensive guide to
844 studying inflammasome activation and cell death', *Nature Protocols*. Springer US, 15(10), pp.
845 3284–3333. doi: 10.1038/s41596-020-0374-9.
846 Tyrkalska, S. D. *et al.* (2016) 'Neutrophils mediate Salmonella Typhimurium clearance
847 through the GBP4 inflammasome-dependent production of prostaglandins', *Nature*
848 *Communications*, 7(May). doi: 10.1038/ncomms12077.
849 Ventayol, P. S. *et al.* (2021) 'Bacterial detection by NAIP/NLRC4 elicits prompt contractions of
850 intestinal epithelial cell layers', *Proceedings of the National Academy of Sciences of the*
851 *United States of America*, 118(16), pp. 1–11. doi: 10.1073/pnas.2013963118.
852 Wada, H. *et al.* (2013) 'Wnt/Dkk negative feedback regulates sensory organ size in zebrafish',
853 *Current Biology*. Elsevier Ltd, 23(16), pp. 1559–1565. doi: 10.1016/j.cub.2013.06.035.
854 Wang, Q. *et al.* (2013) 'Pyroptotic cells externalize eat-me and release find-me signals and
855 are efficiently engulfed by macrophages', *International Immunology*, 25(6), pp. 363–372. doi:
856 10.1093/intimm/dxs161.
857 Wang, Y. *et al.* (2017) 'Chemotherapy drugs induce pyroptosis through caspase-3 cleavage of
858 a gasdermin', *Nature*. Nature Publishing Group, 547(7661), pp. 99–103. doi:
859 10.1038/nature22393.
860 Wang, Z. *et al.* (2020) 'Zebrafish GSDMEb Cleavage-Gated Pyroptosis Drives Septic Acute
861 Kidney Injury In Vivo', *The Journal of Immunology*, 204(7), pp. 1929–1942. doi:
862 10.4049/jimmunol.1901456.
863 Westerfield, M. (2000) *The Zebrafish Book. A Guide for the Laboratory Use of Zebrafish*
864 *(Danio rerio)*. 4th edn. University of Oregon Press, Eugene.
865 Yang, D. *et al.* (2015) 'Caspase-11 Requires the Pannexin-1 Channel and the Purinergic P2X7
866 Pore to Mediate Pyroptosis and Endotoxic Shock', *Immunity*, 43(5), pp. 923–932. doi:
867 10.1016/j.immuni.2015.10.009.
868
869

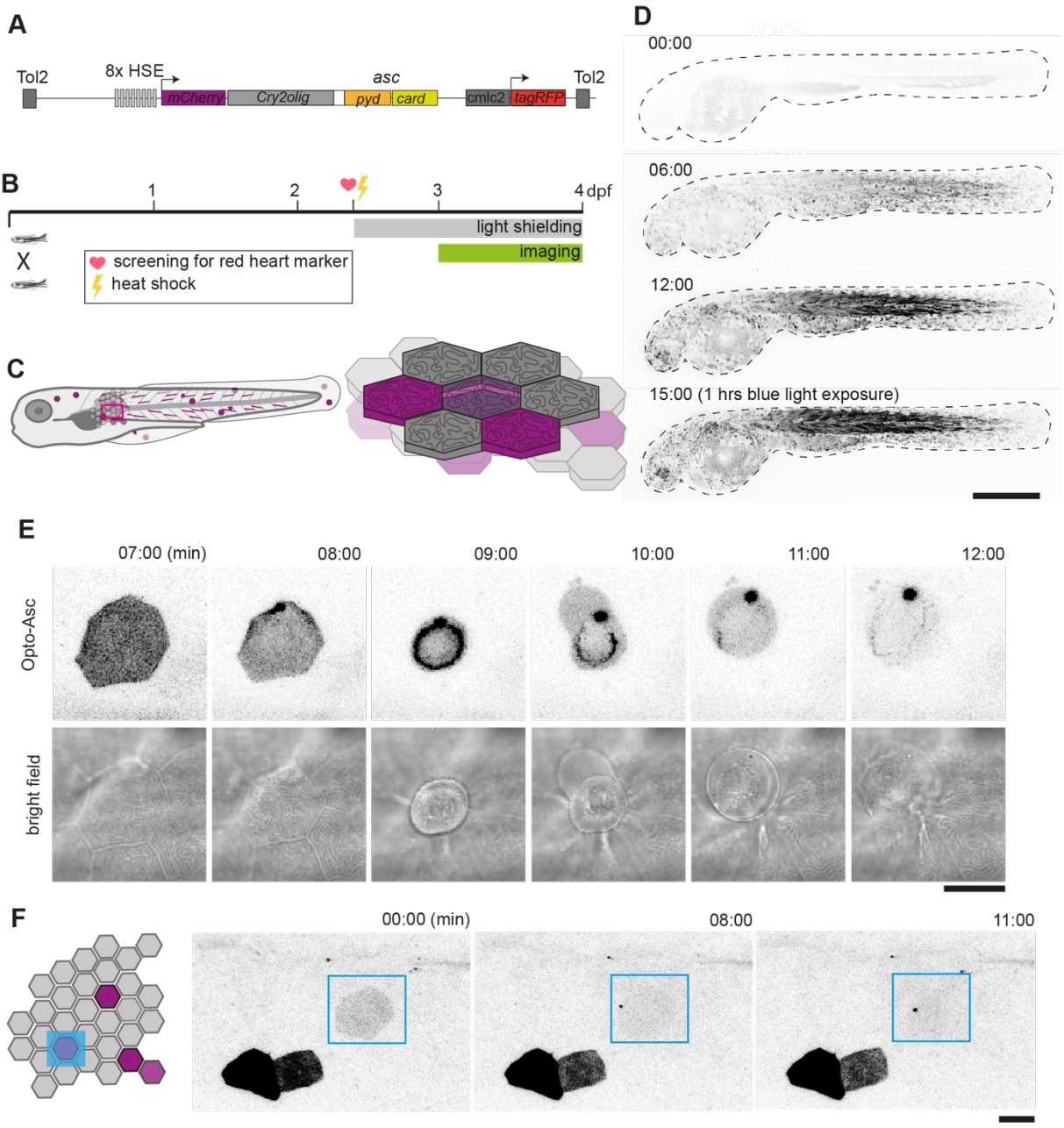

870

871

872 ***Figure 1: Optogenetic tools for Asc-dependent inflammasome formation***

873 **A.** The optogenetic construct (Opto-Asc) consists of a heat shock element placed upstream
874 of a cassette containing the sequences for *mCherry*, the photoactuator *Cry2olig* domain and
875 *asc,* followed by a cassette containing the "red heart" marker cmlc2:*tagRFP*. The two
876 cassettes are placed between Tol2 sites for insertion into the genome.

877 **B**. Experimental set-up: Progeny from the transgenic lines are first screened for the
878 expression of the red heart marker at 2 dpf. Positive larvae expressing cmlc2:*tagRFP*
879 are heat-shocked and kept in dark conditions to prevent spontaneous opto-Asc activation
880 throughout the experiment. Imaging is performed at 3 dpf.

881 **C.** Schematic depicting the stochastic expression of Opto-Asc. Left: overview of larva; right:
882 diagram of the epidermis with the periderm on top (dark colour) and basal cell layer
883 below (light colour).
884 **D.** Time lapse images of 3dpf larva expressing Opto-Asc. Expression of Opto-Asc becomes
885 detectable at 6 hours post heat shock. The frame rate is 15 min, time points are hours after
886 heat shock, scale bar is 200 µm.
887 **E-F**. Example of Opto-Asc forming specks in the epithelial layer of 3dpf larva expressing
888 Opto-Asc. Scale bars are 20 µm.
889 **E.** Time-lapse imaging after 488nm laser illumination of the periderm cells. Top row: Asc-
890 expressing cell forming a speck (t=8 mins). Bottom row: morphology of the dying cell in
891 bright field. Within a minute of speck formation, the cell changes morphology and is
892 extruded. All bright field images are at the plane of the periderm cells; fluorescent
893 images are z-projections 30 planes (z=1 µm)
894 **F.** Local activation of Opto-Asc in a single cell. Diagram of periderm showing four cells
895 expressing Opto-Asc and region of optogenetic activation (blue square). The cell with the
896 lowest expression of Opto-Asc was illuminated by 2-photon laser. Only this cell forms a
897 speck.

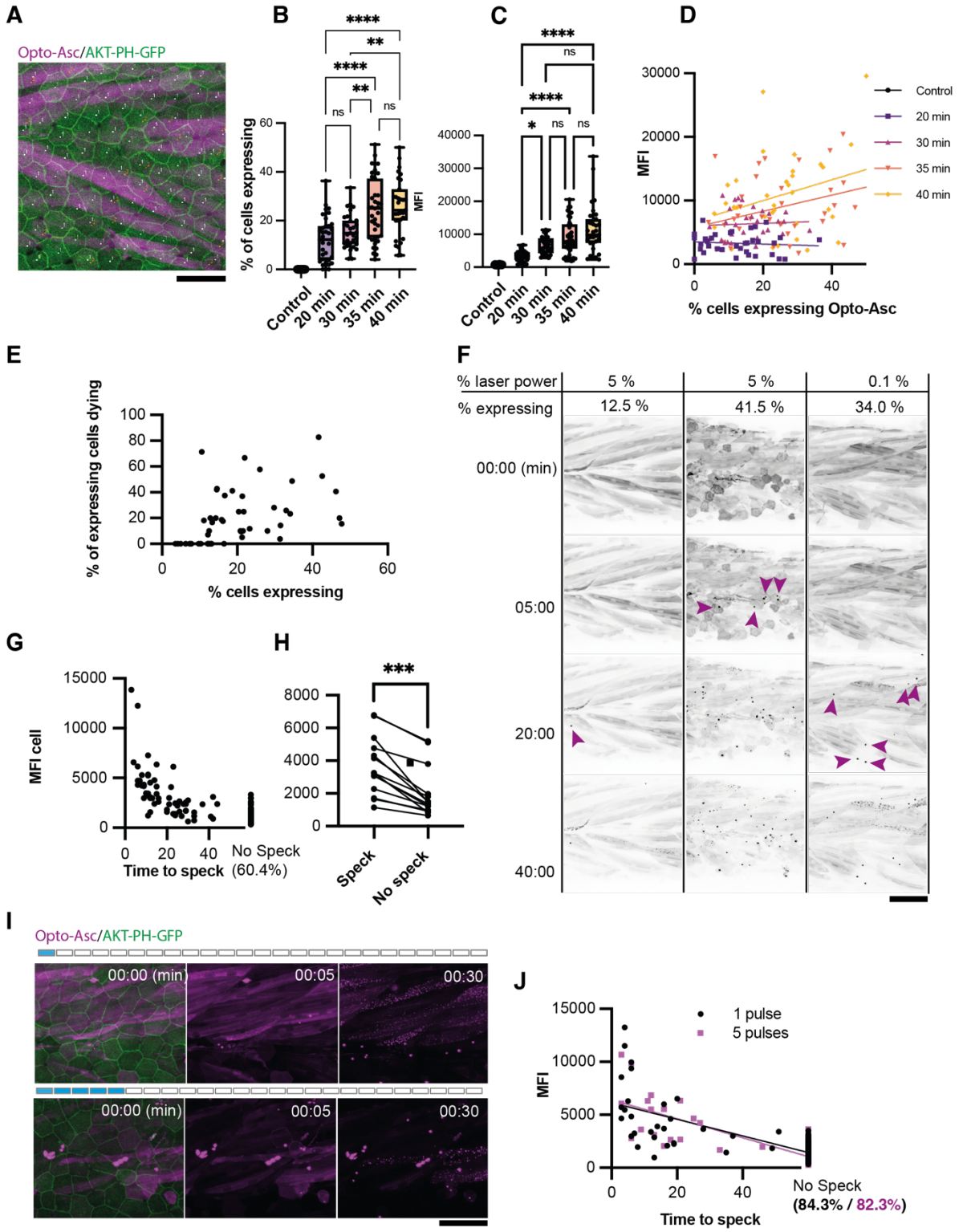

Figure 2: Effect of heat shock and light exposure.

A. Periderm in a larva expressing Opto-Asc (magenta) and AKT-PH-GFP to mark membranes (green) at 16 hr post heat shock (hrpHS). Cells are individually numbered for subsequent quantification of Asc expression. Opto-Asc in this figure is mainly visible in muscles underlying the epidermis, which are seen in this maximum Z-projection. For quantification of

904 Asc-expressing periderm cells, individual z-planes within the periderm are evaluated. Scale
905 bar: 50 µm
906 **B-D**. Dependence of Opto-Asc expression on heat-shock protocol
907 **B.** Percentage of Opto-Asc expressing cells and **C**. overall mean fluorescence intensity (MFI,
908 measured on max projections) in larvae heat-shocked for different time periods (N>29 for
909 each condition; each dot represents one larva).
910 **D.** Correlation between percentage of Opto-Asc-expressing cells and overall MFI for all
911 larvae for each condition measured in B (N=136/>29 per condition).
912 **E.** Correlation between the percentage of Opto-Asc expressing cells and the number of
913 expressing cells dying within 60 min (N=47 movies; each dot one larva); all movies at 1 min
914 frame rate, 5 % relative laser power.
915 **F.** Examples of larvae expressing Opto-Asc after exposure to 488 laser light at different laser
916 powers. The number of Opto-Asc expressing periderm cells (shown as % positive cells) does
917 not correlate strictly with the level of laser power, nor does the expression level in the
918 underlying muscles. If a sufficient number of periderm cells are positive, specks are formed
919 even at low laser power. First appearance of specks is indicated by magenta arrows.
920 **G.** Correlation between MFI of Opto-Asc in single cells and the time from beginning of 488
921 laser light exposure to speck formation. Cells were followed for 60 min; 60.4% of the cells
922 had not formed a speck at this time. N=156 cells from 14 different larvae.
923 **H.** Comparison of average MFI between Opto-Asc expressing cells in individual larvae that
924 form and do not form a speck within 60 min (N=15 individual larvae). The values
925 representing the average MFI for speck-forming and non-speck-forming cells for each larva
926 are connected by a line; $p<0.001$.
927 **I.** Time lapse of Opto-Asc expressing larva exposed to a single or to 5 laser light pulses (1 or 5
928 frames acquired with 488 laser light). Scale bar is 50 µm.
929 **J.** Correlation between MFI of single cells and onset of speck formation in cells exposed to
930 either 1 (red circles) or 5 (black outlined squares) pulses of 488 laser light. Cells were
931 followed for 60 min. N=164 cells in 9 larvae for 1 pulse, N=86 cells in 5 larvae for 5 pulses.

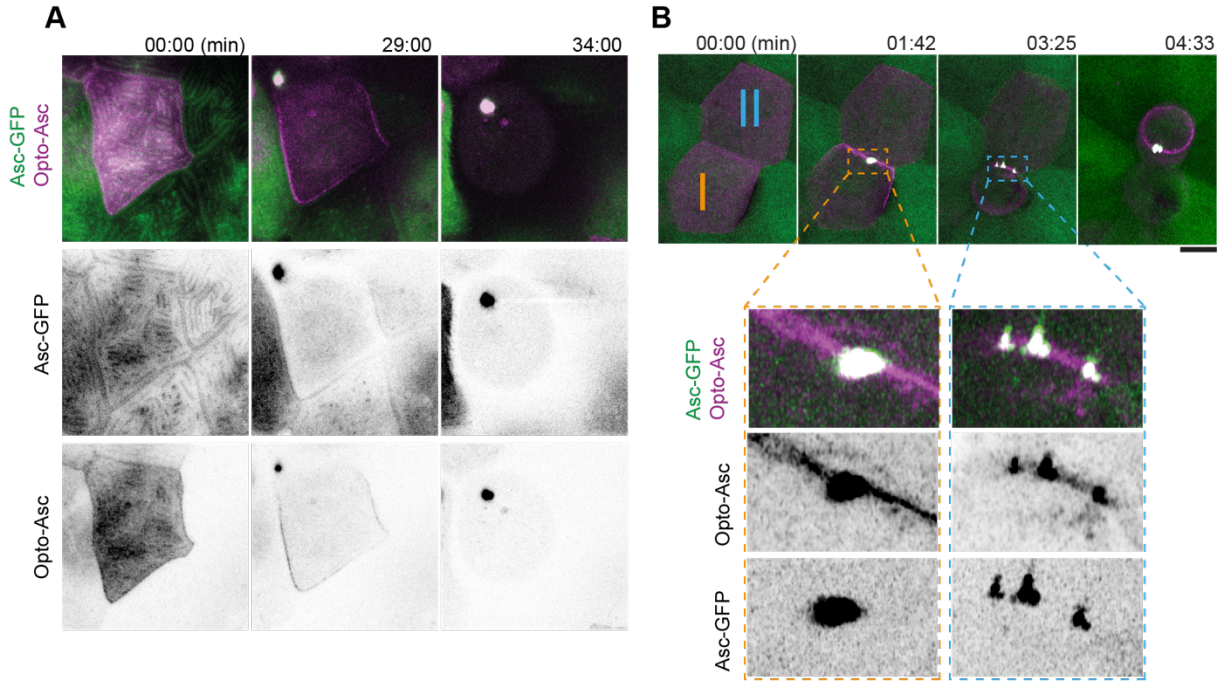

932

933 ***Figure 3: Speck formation dynamics of Opto-Asc and recruitment of endogenous Asc.***

934 **A**. Time lapse of speck formation induced by Opto-Asc (magenta) and recruitment of

935 endogenous Asc (green, ubiquitous) in a periderm cells. Scale is 10 µm.

936 **B.** Two neighboring cells (I and II) forming either a single speck (cell I) or multiple specks (cell

937 II) along the cell membrane. The specks coalesce as the cell shrinks. Scale is 2 µm.

938

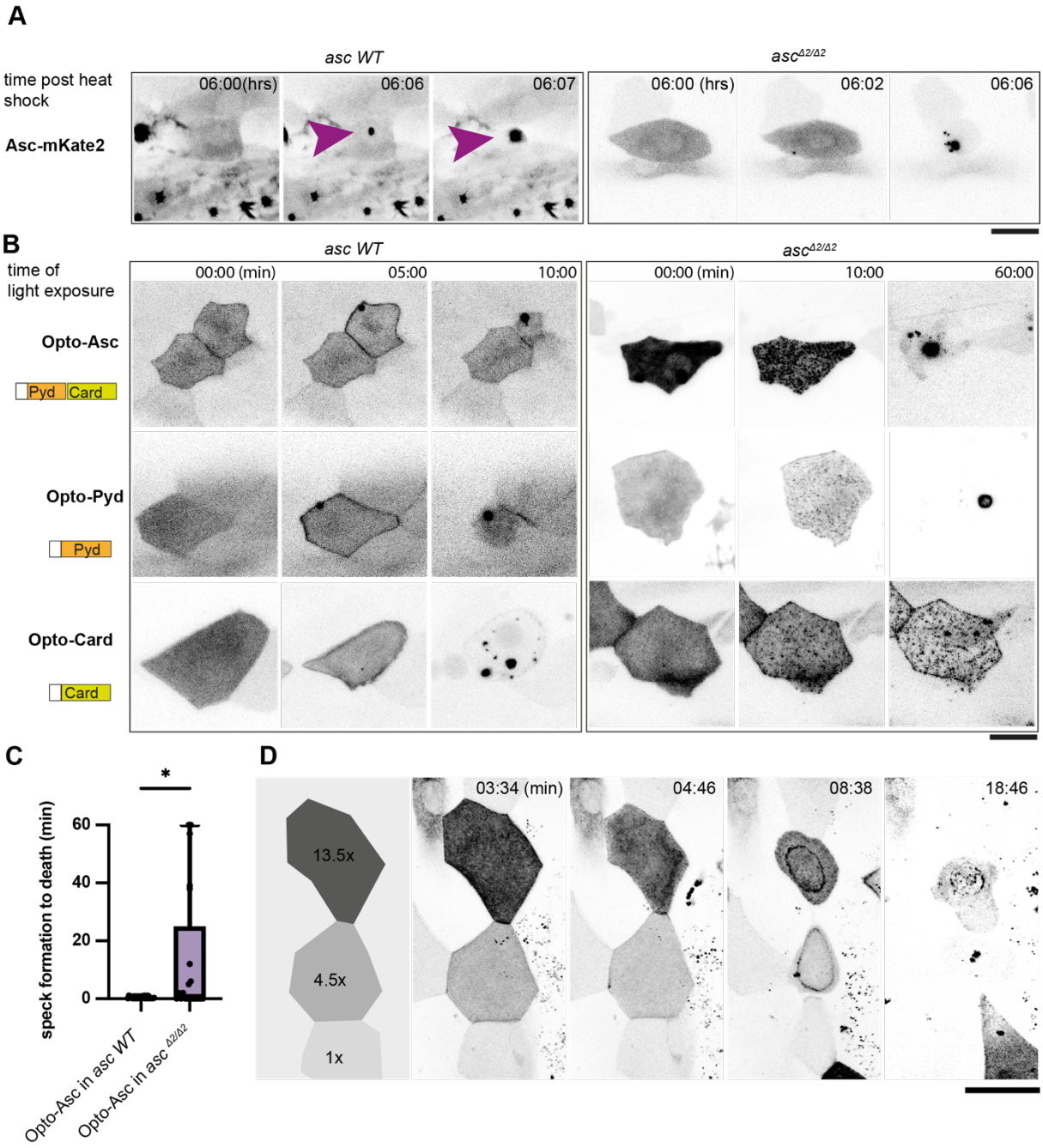

Figure 4: Opto-Asc speck formation and dependence on endogenous ASC.

A, B. Speck formation induced by Asc-mKate2, Opto-Asc, Opto-Pyd and Opto-Card in wildtype larvae and *asc*$^{\Delta 2/\Delta 2}$ larvae. Red frames indicate frames in which cells are dying. Scale bar is 20 µm.

A. Time for Asc-induced specks is counted from end of heat shock. Purple arrow heads mark the speck in the cell of interest. Specks formed by surrounding cells can be seen as balck spots

B. Time is in min counted from the last timepoint before visible speck formation.

948 **C**. Time is measured between first detectable appearance of a speck and first morphological
949 sign of cell death (deformation of cell) in wildtype and *asc*$^{\Delta 2/\Delta 2}$ larvae. *=p<0.05.
950 **D.** Dynamics of speck formation in three cells with different expression levels of Opto-Pyd.
951 Relative intensity levels shown in the diagram on the left are measured in relation to the cell
952 with the lowest level (1x) after background subtraction. Time is measured in minutes; scale
953 bar is 20 µm.
954

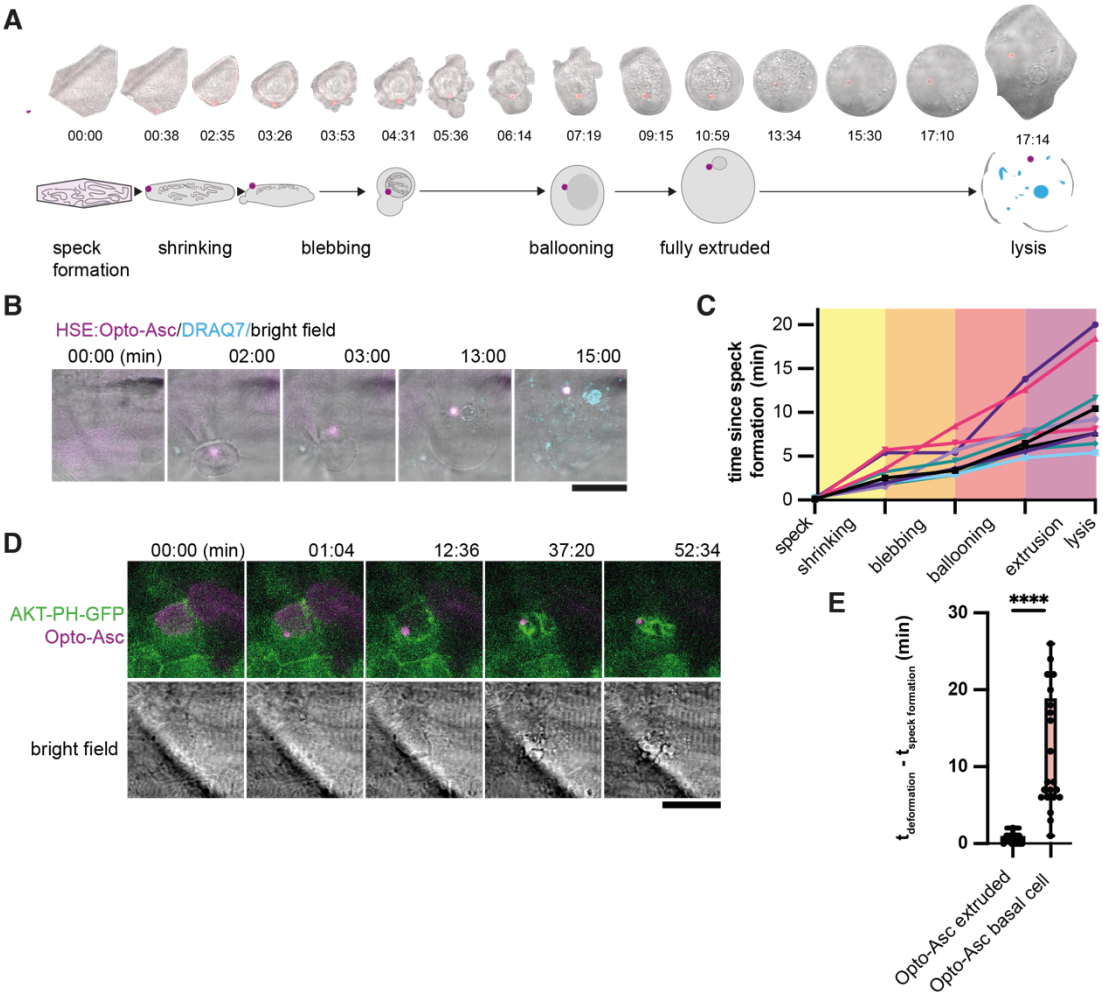

Figure 5: Stages of Asc-speck-induced e extrusion from the periderm.

A. Example of a single cell from a bright-field movie (top) and a schematic showing stages of periderm cell extrusion and lysis after speck formation (bottom).

B. DRAQ7 staining of a cell that lyses after the full extrusion from the periderm. Scale bar is 20 µm.

C. Time lines for 10 periderm cells undergoing the steps of cell extrusion described in A. Time is in minutes.

D. Basal cell dying after formation of an Opto-Asc-speck (magenta). Cell membrane is labeled by AKT-PH-GFP (green)

E. Time between Opto-Asc speck formation and the appearance of first morphological signs of cell death (deformation of cell) in periderm and basal cells. ****=p<0.0001

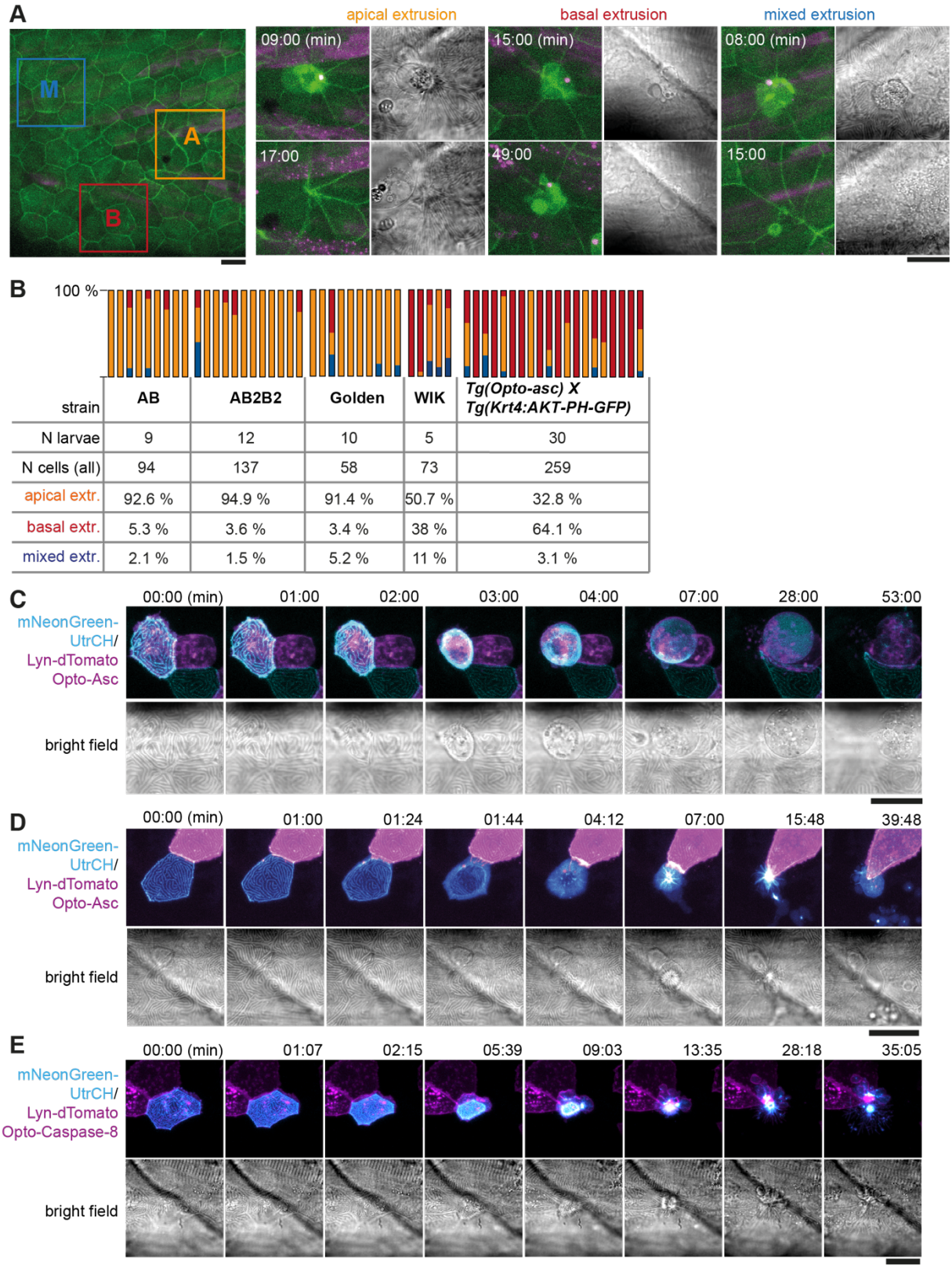

strain	AB	AB2B2	Golden	WIK	*Tg(Opto-asc) X Tg(Krt4:AKT-PH-GFP)*
N larvae	9	12	10	5	30
N cells (all)	94	137	58	73	259
apical extr.	92.6 %	94.9 %	91.4 %	50.7 %	32.8 %
basal extr.	5.3 %	3.6 %	3.4 %	38 %	64.1 %
mixed extr.	2.1 %	1.5 %	5.2 %	11 %	3.1 %

Figure 6: Apical and basal extrusion during Opto-Asc induced cell death

A. Examples of responses to Opto-Asc (magenta) speck formation in three periderm cells within the same larva (marked by blue, orange and red squares in the overview image); cell borders marked by AKT-PH-GFP, green. Dying periderm cells can be extruded apically (orange), basally (blue) or in both directions (red).

974 **B.** Percentage of periderm cells extruded either apically, basally or in both directions (mixed)
975 after Opto-Asc speck formation in different *Danio rerio* laboratory strains and transgenic
976 *Tg(Opto-asc X Krt4:Akt-PH-GFP)* larvae. Each bar represents one larva, the y-axis shows what
977 fraction of cells undergoes which type of extrusion.
978 **C-D.** Response of the actin cytoskeleton in cells that are apically (C) or basally (D) extruded
979 after formation of an ASC speck (magenta). Actin is labeled using mosaic expression of
980 mNeonGreen-UtrCH (cyan). The apical cortical actin ridges can also be seen in bright field
981 images. Membranes of cells are mosaically labeled by expression of lyn-tagRFP (also
982 magenta).
983 **E**. Actin response to Opto-Caspase-8-induced apoptosis in periderm cells; actin in the dying
984 cell is in cyan (mNeonGreen-UtrCH)**.** Membranes of cells are mosaically labeled by lyn-
985 tagRFP (also magenta). Scale bars in all images are 20 µm

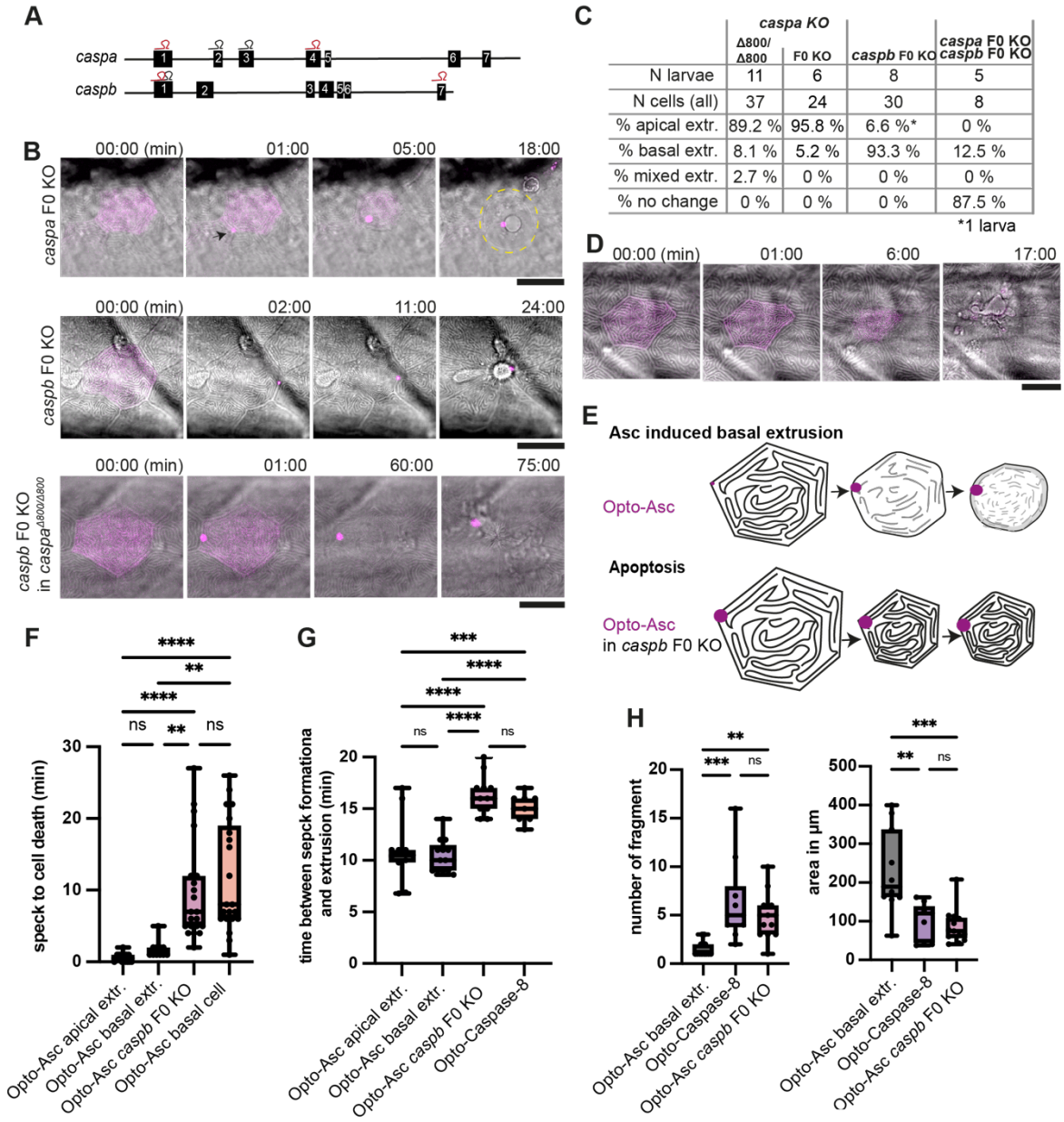

	caspa KO Δ800/Δ800	caspa KO F0 KO	caspb F0 KO	caspa F0 KO caspb F0 KO
N larvae	11	6	8	5
N cells (all)	37	24	30	8
% apical extr.	89.2 %	95.8 %	6.6 %*	0 %
% basal extr.	8.1 %	5.2 %	93.3 %	12.5 %
% mixed extr.	2.7 %	0 %	0 %	0 %
% no change	0 %	0 %	0 %	87.5 %

*1 larva

Figure 7: Inflammatory caspases in cell extrusion and rapid cell death after Asc-speck formation.

A. Schematic of the *caspa* and *caspb* genes and sgRNA binding sites for F0 CRISPR/Cas9 knock-outs (F0 KO).

B. Representative responses of periderm cells after speck formation in *caspa* F0 KO, *caspb* F0 KO and *caspa* F0 KO/*caspb* F0 KO. Scale bar is 20 µm.

C. Percentages of apically extruded and basally extruded cells and cells that do not die within the observation time after Opto-Asc speck formation in different F0 KO backgrounds.

D. Periderm cell dying by apoptosis after Opto-Caspase-8 induction; scale bar is 20 µm**.**

E. Schematic of basally extruding cell after Opto-Asc induction and isomorphic shrinkage as seen in in *caspb* F0 KO larvae after Opto-Asc induction.

998 **F.** Time between Opto-ASC speck formation and first morphological signs of cell death
999 (deformation of cell) in the indicated conditions.
1000 **G.** Time of gap closure after death of single periderm cells which are either extruded or
1001 retained after the indicated treatments.
1002 **H.** Number of fragments at the time of gap closure and area of the largest cell fragment of
1003 retained cells after Asc-Speck formation in WT and *caspb* F0 KO larvae and of apoptotic cells
1004 after Opto-Caspase-8 induction. **F-H.****=p<0.01, ***=p<0.001, ****=p<0.0001
1005

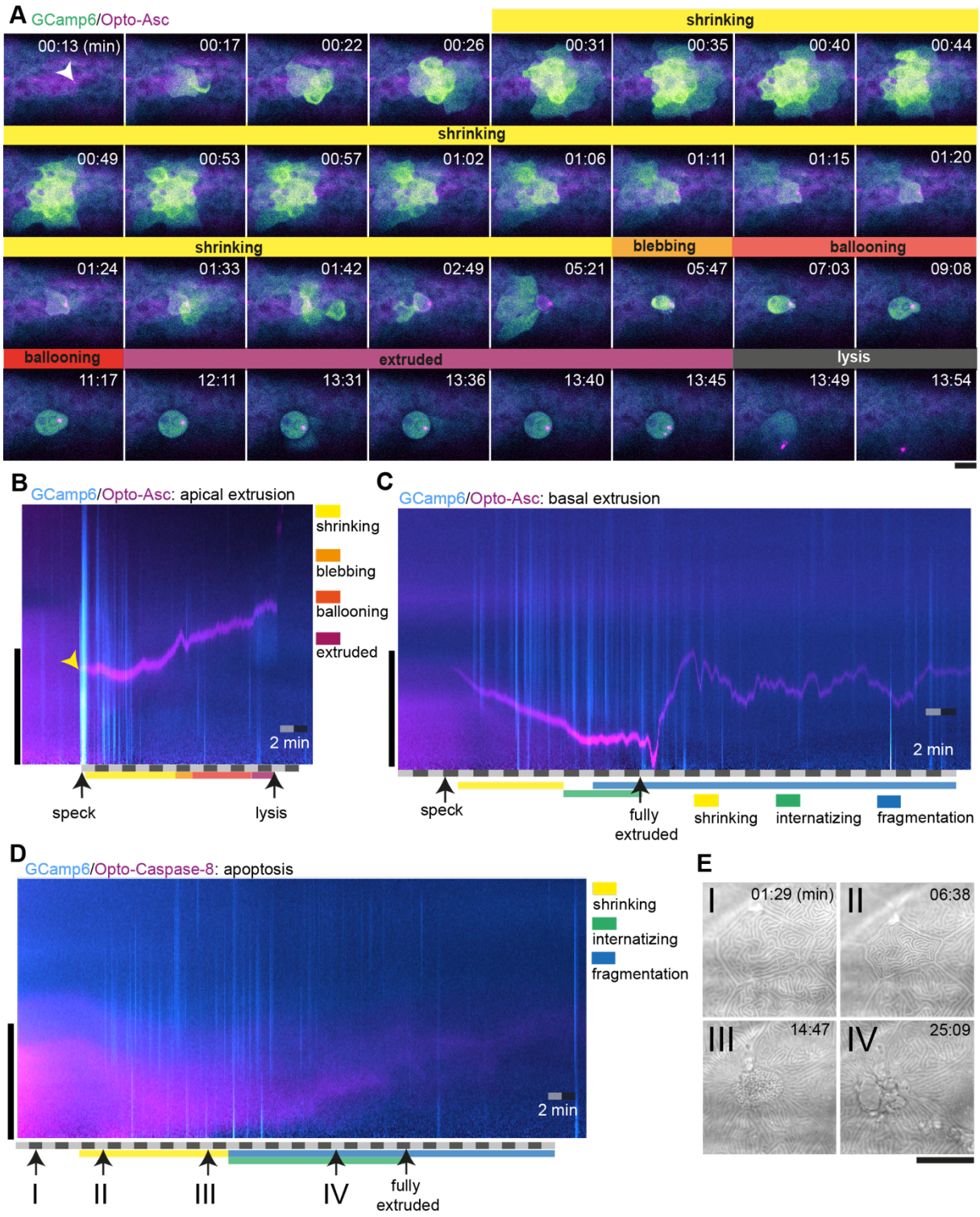

Figure 8: Ca^{2+} signaling in epithelial cells in response to dying cells

A. Example of Ca^{2+} signaling in epithelial cells surrounding a cell forming an Opto-Asc speck (yellow arrow head) and being extruded from the tissue. Frames from a time-lapse image sequence of a larva expressing GCamp6 (light green) and Opto-Asc (magenta). Phases of the extrusion were characterized using the bright field channel, as described in Fig 5 and are color coded (yellow-black). Scale bar is 20 µm.

1013 **B-D.** Two-dimensional representation in time and space (derived from 3D kymographs) of
1014 the Ca^{2+} response to cell death in the larval epidermis. The y-axis shows the radial space
1015 around the dying cell, as described in supplementary figure 7. GCamp6 Ca^{2+} sensor signal
1016 intensity is shown in cyan and Opto-Asc in magenta. The scale bar on the y-axis is 20 µm.
1017 Time is marked along the x-axis in 2min blocks.
1018 **B.** Ca^{2+} signaling response to Opto-Asc-induced apical extrusion as shown in A. The phases of
1019 extrusion are color coded (yellow to dark red) as in panel A and Figure 5C.
1020 **C**. Opto-Asc-induced cell death with basal extrusion. Phases of extrusion marked along the x-
1021 axis.
1022 **D**. Opto-Caspase-8 (magenta)-induced apoptosis. Numbers on the x-axis refers to the images
1023 in E.
1024 **E.** Bright field images of the cell analyzed in D illustrating stages of apoptotic cell death. I:
1025 Cell morphology before the first signs of cell death; II: isomorphic shrinkage of cell; III:
1026 microridge pattern has dissolved and cell starts to internalize; IV: cell has started to
1027 fragment.
1028 Scale bar in all images is 20 µm.
1029
1030
1031